UNIVERSIDAD POLITÉCNICA DE MADRID

ESCUELA TÉCNICA SUPERIOR DE INGENIERÍA AERONÁUTICA Y DEL ESPACIO

GRADO EN INGENIERÍA AEROESPACIAL

TRABAJO FIN DE GRADO

STABILITY OF EQUILIBRIUM POINTS OF ASTEROID 243 IDA APPLYING POLYHEDRAL METHOD TO APPROXIMATE GRAVITATIONAL POTENTIAL FIELD

AUTOR: Aníbal GUERRERO HERNÁNDEZ

ESPECIALIDAD: Ciencias y Tecnología Aeroespacial

TUTOR DEL TRABAJO: Manuel RUIZ DELGADO

Julio de 2022

Dedicated to my dad and Cati for being there all the way.
To my family and friends for making Madrid a second home to me.
In loving memory of my grandmother.

Contents

List of Figures

List of Tables

Chapter 1

Introduction

1.1 Background

Human civilization is programmed to be eternally curious. In the story of mankind, every generation has been eager to explore unknown worlds ever since it became conscious of its own existence. Heading for the stars and pushing the limits has lead the progress of Homo Sapiens in history. Modern technology may seem as a miracle to human ancestors, empowering the general population to explore the mind's full potential and creativity in inexplicable ways. Nowadays, scientists will not limit themselves to looking up into the sky and wander, but employ the Hubble telescope to observe the limits of the observable Universe [1]; the Cassini-Hyugens probe has reached Titan, Saturn's moon, and what perhaps may be mankind's future home [2]; and the space probe Galileo made its greatest discovery when it observed that asteroid 243 Ida has the first ever natural satellite (Dactyl) discovered and photographed [3].Evermore clear sceneries are captured by advancing, sophisticated material, allowing for an increasingly detailed perception of the Solar System. This progress can very fittingly be bookmarked by the discovery of asteroids. No longer than two hundred years ago none would have thought that our Solar System was home to more than the Sun and eight completely isolated orbiting planets at astronomical distances from one another. From the beginning of the nineteenth century, Solar System small bodies gradually appeared in the void of space, where never before had they been seen. Important properties such as their weight or size could not be determined at that time. As humans advanced to the twentieth century, they had learned that the total mass of the observed small bodies was tiny compared to the mass of the planets, leading to a decline in the number of studies in that spectrum. [4]. During the space missions taking place from 1920 to 1970s, their chemical composition and general interior of the small bodies had been studied in depth. A number of asteroids' shapes have been determined and some have been imaged by radar observations and by spacecrafts with high resolution respectively. These images represent abundant geomorphic features of the surfaces, making each unique in shape and size [5]. Nowadays it is determined that Solar System small bodies

most likely contain information on the origins of how life on Earth started and our neighbor planets, leading to a profound shift of modern view of nature [6, 7]. These small bodies have a deep impact on the development of multiple related industries e.g. aerospace engineering, space industry, cosmo-biology, planetary geology, etc.

Solar System small bodies are all the natural objects orbiting the Sun other than dwarf and normal planets. The majority in this group can be encompassed as all the asteroids distributed between the planetary orbits. Giuseppe Piazzi was the one who discovered the first asteroid, 1 Ceres. After two centuries and over 380,000 asteroids later, 1 Ceres is known as the largest member of the asteroid belt. Approximately, 95% of the asteroids have been discovered over the last decades [8]. As technology has advanced through the last century, missions targeting asteroids and other small bodies have evolved from remote sensing observations, to flyby, rendezvous, in situ explorations and return missions. Asteroids have become one of the main targets within deep space exploration. Studying an asteroid proves to be highly complex, as it requires a plethora of skilled techniques such as orbital tracking, autonomous navigation and control of spacecrafts, and global trajectory optimization. Therefore, it results in an extensive measurement of the national comprehensive power and will determine in great detail the future of national space defence strength, international strategic balance, space resource sharing, and space infrastructure. More so, the private space industry is adventuring into the resource exploitation of asteroids, for further future development of Earth platinum group metal (PGM) and hydrogen markets, as well as developing space infrastructure that could host space tourism, extraterrestrial bases, and anything humans can imagine.

The asteroid hunt commenced back in the early 20^{th} century. From 1920 to the 1990s, various space missions were proposed for SSSB exploration. The efforts continue until this day, as asteroids have been proven to be of great importance when addressing academic questions on how our Solar System was formed, the origin of planet Earth, and lucrative opportunities through mineral extraction in a deep space mining environment. To grasp some of the most important missions accomplished until this date, a mission chronology of Solar System Small Body explorations Table 1.1 has been created. The most crucial missions have been compiled, organized into the spacecraft utilized, mission name, launch and arrival time, flight duration, and additional notes regarding the mission.

The first attempt to reach an SSSB occurred in January 1989, when Phobos 2 achieved Mars orbit [9, 10]. As the probe was in the approach phase and about to deploy the lander, contact was lost on 27 March 1989. Meanwhile, NASA's unmanned spacecraft Galileo visited two asteroids en-route to Jupiter: 951 Gaspra in October 1991, and 243 Ida in August 1993 [11, 12, 13]. The spacecraft measured the shape, size and surface craters of both. It also discovered that the asteroid 243 Ida was a binary system with a smaller Dactyl orbiting around it. Refer to Fig. 1.1b. In February 1996, NASA launched Near Earth Asteroid Rendezvous (NEAR) spacecraft [14, 15, 16]. The NEAR spacecraft made the first multi-spectral images of C-type 253 Mathilde and successfully improvised a landing on near-Earth asteroid

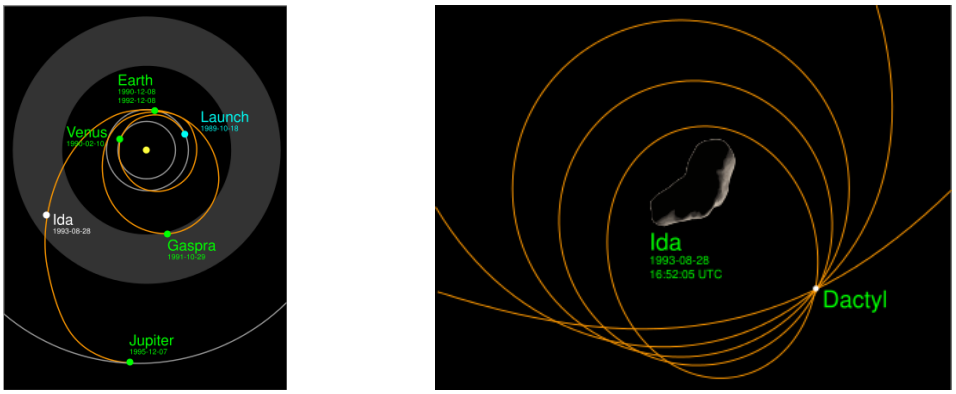

(a) Diagram of Galileo's spacecraft path and encounter with asteroid 243 Ida. [11]

(b) Diagram of asteroid 243 Ida-Dactyl binary system and Dactyl's possible orbits. [13]

Figure 1.1: Galileo mission, asteroid 243 Ida and 1 Dactyl.

(NEA) 433 Eros. In October 1997, Cassini orbiter and Huygens Titan lander orbited Saturn, performing repeated by-flights of Saturn's moons [17, 18, 19]. Huygens Titan lander was the first probe to land on a satellite of another planet. Deep Space I probe flied by asteroid 9969 Braille and comet Borrelly in 1998 [20]. The probe successfully detected coma plasma and gas streams on the nucleus. JAXA launched the Hayabusa mission in May 2003, targeting asteroid 25143 Itokawa [21, 22, 23, 24]. The spacecraft was developed to return a sample of material for further analysis. The probe made a rendezvous with the asteroid in September 2005, landing on its surface two months later, and finally returning the collected samples back to Earth in 2010. Rosetta orbiter and Philae lander launched in 2004 and accomplised orbit and landing on Comet 67P/Churymov-Gerasimenko [25, 26, 27, 28]. Later, NASA developed the Deep Impact Impactor in 2005, which mission was to aim for a kinetic impact test on the nucleus of Comet 9P/Tempel [29, 30, 31]. Through the kinetic impact, the ejecta and shape was to be measured, along the depth of the crater. In September 2007, NASA launched another spacecraft named Dawn [32, 33, 34, 35, 36]. Dawn's mission was to visit asteroids 4 Vesta and 1 Ceres. A common effort between ESA and JAXA was executed to deploy the Hayabusa 2, as a follow up mission for the Hayabusa, in December 2014. It carried MINERVA-II rovers and a MASCOT lander to asteroid 162173 Ryugu [37, 38, 39, 40]. Finally, NASA launched in September 2016 OSIRIS-REX Project, in order to send a spacecraft to asteroid 101995 Bennu and return samples to the Earth [41, 42].

Another mission worth mentioning is the Chinese lunar probe Chang'E 2. The probe made a close flyby with NEA 4179 Toutatis in December 2012. Close-up imaging of Toutatis' surface was achieved, making China the fourth space agency to conduct a successful mission to an asteroid [43].

Spacecraft	Destination	Launching Time	Arrival Time	Flight Duration	Notes
Phobos 2 Orbiter and Lander	Mars and Phobos	12 July 1988	29 January 1989	202 days (6mo, 18d)	Phobos 2 achieved Mars orbit, but contact was lost on 27 March 1989 shortly before Phobos approach phase and deployment of Phobos landers
Galileo and Space Shuttle Atlantis STS-34	Asteroid 951 Gaspra	18 October 1989	29 October 1991	741 days (2y, 11d)	Incidental flyby enroute to Jupiter.
Galileo and Space Shuttle Atlantis STS-34	Asteroid 243 Ida	18 October 1989	28 August 1993	1410 days (3y, 10mo, 10d)	Incidental flyby enroute to Jupiter. Dactyl discovery.
Near Earth Asteroid Rendezvous (NEAR)	Asteroid 433 Eros	17 February 1996	14 February 2000 entered orbit. 12 February 2001 landed.	1459 days (3y, 11mo, 29d)	The orbiter performed an improvised landing on Eros. Its mission ended 28 February 2001.
Cassini orbiter and Huygens Titan lander	Saturn and Titan	15 October 1997	1 July 2004 entered orbit 14 January 2005 Huygens landed on Titan	2452 days (6y, 8mo, 17d), 2649 days (Huygens), (7y, 3mo)	Mission ended 15 September 2017. Saturn orbiter, performing repeated by-flights of Saturn's moons; also deployed the Huygens Titan lander, the first probe to land on a satellite of another planet.
Hayabusa and MINERVA	Asteroid 25143 Itokawa	9 May 2003	12 September 2005 matched velocity with Itokawa, 19 and 25 November 2005 landings	858 days (2y, 4mo, 4d)	The MINERVA hopper was lost on 12 November 2005. Hayabusa's return journey to Earth began in April 2007; the spacecraft returned to Earth 13 June 2010.
Rosetta orbiter and Philae lander	Comet 67P/ Churyumov-Gerasimenko	2 March 2004	6 August 2014 Entered orbit, 12 November 2014 Philae landed	3907 (10y, 8mo, 10d)	64 Hours data transmission. Lander reactivated for 85 seconds 13 June 2015. Controlled impact to end mission on 30 September 2016.
Deep Impact Impactor	Comet 9P/Tempel	12 January 2005	4 July 2005 impacted Tempel	174 days (5mo, 23d)	First probe to directly impact a comet.
Dawn	Asteroid 4 Vesta	27 September 2007	16 July 2011 entered orbit	1388 days (3y, 9mo, 19d)	Departed Vesta for 1 Ceres on 5 September 2012.
Dawn	1 Ceres	27 September 2007	6 March 2015 entered orbit	2718 days (7y, 5mo, 8d)	Last contact 31 October 2018.
Hayabusa2 with MINERVA-II rovers and MASCOT lander	Asteroid 162173 Ryugu	3 December 2014	27 June 2018 matched velocity with Ryugu, 21 February 2019 landing	1541 (4y, 2mo, 18d)	N/A
OSIRIS-REX	Asteroid 101955 Bennu	8 September 2016	3 December 2018	816 days (2y, 2mo, 25d)	Orbiter and Sample Return.

Table 1.1: Solar System Small Body Mission Chronology [9] - [42].

1.2 Academic Merits and Significance

Solar System small bodies exploration is of great importance in multiple aspects. Asteroids and other small celestial bodies were formed as residuum when the Solar System was in its early formation stages. Contrary to planets, these asteroids did not participate in the process of planetary evolution. Therefore, they could provide vital information on what happened at the origin of the planets, and the start of life [44]. Not also are small bodies a possible door to our past, but they also are very rich in mineral resources. For example, a rather common sized M-type asteroid of 1km is said to contain several times the amount of rare metals found on Earth. Some of these rare metals are: nickel, platinum, cobalt, iridium, among other platinum group metals (PGMs). Mining on an asteroid has been extensively proposed and discussed as part of the future in space engineering. Companies such as Asteroid Mining Corporation, based in the United Kingdom, are working towards redefining mining.

Their focus is to tap into these sources of PGMs, which are key ingredients in a range of modern technologies that range from hydrogen cars to smartphones and prosthetic limbs. By developing the technology necessary, a brighter and more sustainable future holds for Earth as mining operations are highly resource-intensive, produces high quantities of byproducts and requires large amounts of water [45].

Lastly, the most practical reason to raise concern on SSSBs is due to their potential to be a threat to planet security. If involved in mutual collisions or the effects of secular perturbations, an NEA's orbit can be altered resulting in the impact of a massive member of these perturbed objects against the Earth. Such event would result in the termination of human civilization with uttermost certainty. However unlikely the event seems, history has taught its lesson. A meteorite impact ended the

dinosaurs' reign, marking the end of the Cretaceous period. Other more recent examples are the Tunguska Event in the early twentieth century, and the Chelyabinsk impact on February 2013. The latter caused extensive property damage and injured over 1500 people. Therefore, learning the impact hazard an asteroid presents, discovering possible NEA threats and how to mitigate them, should be a priority as it will become the first avoidable natural disaster [46].

In situ exploration and sample return missions of SSSBs provide vital data and evidence to scientific researches while proving new technologies in real scenarios and harsh environments, pushing further resource and development. It can also be used for NEA deflection due to its contribution in the estimation of the target's parameters, ensuring an accurate implementation of the actions executed to deflect the asteroid. Therefore, proving irreplaceable to remote sensing and observation. Sending probes to NEAs proves a great challenge to the responsible bodies involved in the mission. More so, excluding requirements on deep space orbital tracking and the vehicle's autonomous navigation, solely the flight dynamics around an SSSB becomes extremely complex due to the surrounding complex mechanical environments. Missions will have to be designed and planned meticulously to accommodate the complexities presented. From the asteroid missions already accomplished stated in Table 1.1, some were not completely successful. For example, as the Hayabusa spacecraft was approaching asteroid 25143 Itokawa in November 2005, it released the surface rover MINERVA at $\sim 1.4km$, attempting to land on the surface. The rover failed to reach the surface due to an error in the predicted trajectory. With post-mission analysis, it was determined that the error was caused to an inaccurate estimation of the asteroid's gravitational field. As another example, during the design of the Dawn mission, the Planetary Science Institute in Tucson demonstrated a possible conflict for the spacecraft. The spacecraft could be trapped in a band region formed by the resonance of Vesta's rotation and the spacecraft's orbit [47], meaning it could not escape with the propulsion system the spacecraft carried. The effect was taken into account during the orbital design of the mission, and the threat was avoided.

Orbital dynamics around small bodies in general prove to be very complex. This complexity mainly arises from two aspects. First, the complex nature of this problem. Solar System small bodies vary in shape, interior structures, chemical composition, mechanical properties, and accordingly the gravitational field around these small bodies could be diverse and irregular for each different SSSB. Second, due to the limitations presented in the technologies utilized for measurements. Therefore, a spacecraft cannot obtain a complete assessment before approaching to the target small body. Some of these characteristics are the shape model, the gravitational data and the rotational state. Corrections and measurements must be taken simultaneously during approach, increasing the complexity and risk of the mission. For these reasons, orbital behavior around SSSBs is significantly different from that around planets and other bigger celestial bodies, like stars. Furthermore, SSSBs have a reduced mass, meaning that the asteroid is under the influence of space perturbations and cannot be neglected, due to its relative influence. Some of these space perturbations include the tidal forces from the Sun and Solar System planets,

and radiative forces. All perturbation forces contribute to the plethora of orbital behaviors presented around small bodies. Some internal mechanisms are still hidden to our knowledge, presenting further challenges to orbital design and control.

The importance of understanding orbital dynamics around a small body becomes obvious. As previously stated, motion control of spacecraft around small bodies is unavoidable for in situ exploration. Furthermore, the geological evolution of individual asteroids (i.e., shape, interior structures and surface features) and the formation of SSSB systems (i.e., binary systems and other asteroid families) proved strong correlation with the orbital behavior in their proximity [48, 49]. Not only will the study of orbital dynamics help finding a driving model for the evolution of the Solar System, but also the intrinsic reasons behind the phenomenons. A theoretical framework of the behaviors of a general nonlinear system has been established. Taking a mass point moving under the influence of an irregular gravitational field is regarded as the typical model of the practical system. It presents a new frontier in modern celestial mechanics to be explored.

1.3 Research Status Survey

A massive study on the orbital dynamics around Solar System small bodies kicked off mid twentieth century, as a result of NASA's asteroid exploration efforts. Initially, the orbital design, motion control and dynamical environment analysis of the spacecraft were condensed to the field of astrodynamics. Simultaneously, planetary physics and celestial mechanic researchers commenced around the intricacies of SSSB formation and evolution, combining various results from ongoing observations. Accordingly, asteroid exploration progress motivated academic interest of nonlinearity researchers. These researchers directed an effort towards studying the dynamical behaviors in special irregular gravitational fields, aiming towards a practical application with asteroids. Thus, this section summarizes the progress and current status of the research fields specified.

1.3.1 Astronautic Dynamics

Orbital dynamics around small bodies revolves around the induced gravitational field of irregular massive bodies. Usually, researchers begin with the applied characteristics of the problem - the approximation of the asteroid's irregular gravitational field. A classic method utilizes spherical harmonics to conveniently describe the gravitational field [50]. Spherical harmonics expand the objective field as spherical harmonic series based on a central item to approximate its non-spherical perturbation. The volumetric integral that determines the potential over the central body is converted to a surface integral, and finally reduced to a series of harmonic coefficients C_{nm} and S_{nm}. These coefficients determine the geometric properties of the objective field. This method provides a uniform formulation for an arbitrary central body [51], proving linear to the harmonic coefficients. When linearity is demonstrated, it enables the values to be identified from past flight data records. Therefore, this method was held as the general go-to technique in calculating the near-Earth orbits of satellites. Going back to the 1920s, extensive academic efforts

went to inversion algorithms of harmonic coefficients [52, 53, 54]. Nevertheless, the spherical harmonic method proved its limitations through the position evaluated with respect to the reference sphere, i.e. the closer the point is to the reference radius on the exterior of the reference sphere, the slower the convergency will be, failing completely if the point is inside the sphere [55]. As the scientific community learned about the method's limitations, Bierly, Hobson and MacMillan proposed the ellipsoidal harmonic method [56, 57, 51]. This new method proposed a reference triaxial ellipsoid as the envelope of the central body, and solves the harmonic coefficients of different degrees and orders according to the three semi-axes. It is capable of providing a wide region of convergency closer the the irregular body studied. Asteroids tend to be more irregular than spherical, meaning that the ellipsoidal harmonic method was a more fitting evaluation of the harmonic coefficients and the study of orbital dynamics around small bodies [58]. For asteroids with an inaccurate determination of their shape, it can be described as triaxial ellipsoids directly, deriving the potential and gravity analytically [59]. This proves more fitting for the small bodies studied. Friedlander, German and Scheeres et al. analyzed particular forms of orbital motion around a rotating ellipsoid [60, 61].

Prior harmonic methods were a great beginning to study the modeling of a gravitational field of an irregular small body, but an asteroid space mission requires an accurate estimation of the gravitational field. Gravitational fields have great reliance on the dimension and shape of the studied body. Therefore, using a sphere or an ellipsoid as an estimation of an asteroid's body is insufficient to correctly asses its gravity. A different but straightforward approach is to describe the mass distribution of the body as a homogeneous polyhedron. The gravity from the small body will be expressed as a volumetric integral over the polyhedron. Through what is from now on referred to as "polyhedral method", explicit expressions of the gravity and potential are derived following conventional routines. The method dates back to the end of the twentieth century [62], but could not be executed until recent decades due to the development of the required computing technology. In 1993, Werner derived the analytical forms of the exterior gravitation of a constant-density polyhedron [62], while Scheeres et al. applied this polyhedral method to orbit studies around asteroid 4769 Castalia [63]. Use of the polyehdral method gained momentum through the years for asteroid mission analysis, becoming the new standard. Meanwhile, Forsberg proposed a new method to approximate the gravitational field of any given body proposed as a non-homogenous polyhedron, i.e. polyhedron divided into multiple unit tetrahedrons with varying densities assigned [64]. Simultaneously, Petrovic and Pohanka et al. reformulated the polyhedral method expressions, suiting them to programming [65, 66], with Tsoulis et al. determining the singularity conditions of these new formulas [67]. The polyhedral method has become the most mature and effective approach to deal with orbital dynamics around small bodies (asteroids). This method is later discussed in Chapter 3 - Modeling Orbital Dynamics in the Potential of Solar System Small Bodies.

On the one hand, the conventional perturbation method is still used in classic orbital theory to study the effects of non-spherical bodies and other items of perturbations around a small body. On the other hand, the equations utilized for orbital motion

near asteroidal gravitational fields is similar to the circular restricted three-body problem (CRTBP). CRTBP has been one of the main topics in astronautic mechanics in the last century. Some methods and conclusions from CRTBP can be extrapolated into our problem. During the twentieth century, Scheeres et al. modeled the gravitational field of some specific asteroids with the polyhedral method, and analyzed the orbital behaviors nearby these SSSBs [63]. Scheeres et al. used asteroid 4769 Castalia as it had a radar shape model, to show the motion equation has a generalized energy integral, existence of equilibrium points, zero-velocity surfaces and Hill region definition analogue to CRTBP definitions [68]. Scheeres et al. also discovered several periodic orbits around Toutatis using the polyhedral method [69]. Hu and Scheeres built up on Toutatis' findings, presenting possible periodic motion in the equatorial plane using the gravitational field of second degree and order [70]. Meanwhile, Antreasian et al. applied the averaging method, with the second degree and order gravity, seeking stable motion around asteroid 433 Eros. A family of retrograde orbits was found [71]. Other perturbations have been studied more in depth, showing how solar radiation pressure and tidal forces from large objects from the Solar System can affect the stability of the spacecraft's orbits around the target asteroid.

SSSBs are distinguished by their diversity in physical properties. These small bodies have different size, shape and components, providing further challenges for in situ explorations. Previous missions such as the ones listed in Table 1.1 have provided precise physical properties of specific asteroids. The obtained data has been used for a detailed estimation of the dynamical mechanics around them. Schemes and Williams et al. analyzed the complete orbital motion near asteroid 433 Eros, based on the data obtained from the NEAR spacecraft. Results proved how conditional the stability of retrograde motion is near the asteroid's equatorial plane, proving important for the mission design [72]. Later, the Hayabusa spacecraft assessed asteroid 25143 Itokawa obtaining a high-resolution model of the asteroid's shape. Scheerees and Gaskell et al. then studied the gravitational properties of the model taking constant-density as the general assumption to discuss the dynamical environment both on the surface and in orbit [73]. Further literature also detailed a trajectory under a close approach to the asteroid's surface, proving a reliable methodology [73]. Simultaneously, the beginning of Dawn's mission demonstrated the importance of the 1:1 resonance with various gravity models, showing the risky working conditions for the spacecraft. IT was later considered into the flight mission design [47]. In conclusion, a detailed estimation of the dynamical environment around asteroids is important both for academic research in astronautic dynamics and future asteroid mission designs.

In the same manner, orbital dynamics around small bodies is vital to the motion control of a spacecraft. Independently of the task commended (companion, hovering, orbiting, approaching, landing, touchdown, sampling, etc), an accurate dynamic model is necessary before the application of a control scheme. Active control strategies and hovering control laws were studied by Broschart et al. Perturbation equations were numerically simulated for stability regions identification. A stable region of body-fixed hovering was found to be approximated to the body's resonance

radius [74]. Asteroid 433 Eros' landing NEAR mission design is discussed in [75]. The landing scenario was detailed through radio metric, optical landmark and laser ranging tracking data. It allows to determine the landing characteristics within the expected margin errors. Braun and Lantoine developed a computational technique for an optimal autonomous controlled soft landing in an irregular gravitational field of a rotating asteroid. The complexity of the environment and the numerical method to solve the control problem was presented. Asteroid Vesta and Golevka were used as examples, identifying the best mission design scenario for each, and uncertainties of the landing process [76]. Landing site selection is crucial too. Constraint conditions in landing site selection such as, landform ,lighting conditions, communication, technical obstacles and scientific merit, etc were presented in [77, 78]. Motion control of a surface rover studied the launch speed, dependent on the geomorphology of the asteroid in [68, 73].

1.3.2 Planetary Science

In the past two decades, planetary scientists have shown an increased interest in binary asteroid systems. The first hypothesis arose two centuries ago, when asteroid Ceres was discovered and suggested to have a Moon. The first and most important discovery was done by the Galileo probe in 1993. It flew past asteroid 243 Ida and found it had a satellite later named Dactyl, confirming the existence of the binary asteroid [79]. Presently, over 200 binary asteroids have been discovered. Binary asteroid systems are important, as they provide information regarding mass and density of each asteroid, providing clues to further understand planetary system dynamics [80]. Besides, Scheeres et al. analyzed stable orbits around under highly non-spherical perturbations, to find natural satellites [81, 82]. It was later introduced a full two-body model for binary orbits studies by Scheeres and Bellerose [81, 83]. As seen from [84], Maciejewski found the absolute and relative motion equations of the two-body model, discussing possible equilibrium phases. Scheeres then studied the stability conditioned of an ellipsoid-sphere model [81]. Even though a binary system is composed of a relatively massive body compared to the orbiting body around it, both exert gravity. The calculation of mutual gravity and potential has been extensively discussed [85, 86]. A better approach was presented in [87, 88], being the two bodies discretized into mass point clusters, and calculating the gravity and potential by summing up that between the mass points. This method showed a slow convergence, meaning a computationally expensive execution. Werner and Scheeres then proposed a method to approximate the mutual gravity based on the polyhedral method [89]. It proved a better convergence and was later applied to future research. It was later encountered that traditional integration methods may lead to simulation problems of the two-body system with precision. Fahnestock and Lee et al. improved the accuracy and efficiency [90, 91], and applied it to study the motion of the binary asteroid system 66391 1999K W4.

The evolution of the geologic features from a small body is complex and involves abundant dynamical phenomenons that affect its orbital behaviors. For instance, asteroids take many micro-meteorite impacts [92], leaving a trace in the form of a crater for a prolonged extension of time [93]. From the asteroid's ejecta, some will be able to escape the asteroids vicinity, while other will be trapped in a tempo-

rary orbit around the asteroid [94], leaving the rest to fall back to the surface and re-accumulate. Research on ejecta can be found from [95]. The NEAR spacecraft opened new interests on the formation of some geological features, as they have been linked to ejecta [96]. Meanwhile, Hamilton and Burns analyzed boundaries of stable orbits around an asteroid, pretending to understand the stability zones [97, 98]. Ejecta motion and the influence solar tide has in it, was studied by Chauvineau et al. [99], while Richter et al. discussed the orbital features of ejecta close to the stability limit [100, 101]. Scheeres and Chauvineaus researched and proved the main differences in the surroundings of a small body, compared to that of planets [102]. Further work for asteroid 243 Ida was detailed. The study on the orbital motion of ejecta from crater Azzurra proved that the re-accumulated ejecta drastically changed the optical features of the northwest part of the asteroid's surface [87]. The study proved the power of a detailed dynamical model to explain real astronomical phenomenons. In the same manner, Durda et al. built the tracer model of ejecta dynamics around asteroid 433 Eros. If combined with surface images, the data can be used to back track the source craters, finding specific historic impact events [103].

Double craters are a special geological formation that is studied widely through recent years [104]. It consists of two craters close or adjacent, showing a similar geological age. Research hypothesizes that the formation of these double craters arise due to a meteorite being disrupted during rendezvous with the asteroid, separating it into two parts and impacting the asteroid's surface at a short interval [105].

1.3.3 Nonlinear Dynamics

An important nonlinear system is a particle in a gravitational field. For planets, a conventional perturbation analysis on its potential provides a complete result, whereas gravitational fields of small bodies demonstrate a wide diversity and are geometrically complex objects. Complex geometries lead to more variety in orbital behaviors. Asteroid exploration missions from the last century pushed academics to study nonlinear dynamics under special backgrounds.

When simple geometries are presented, gravitational fields can be adopted as the abstract models. For example, Halamek used a line segment to approximate the elongated objects [104]. Then, Prieto-Llanos et al. found the equilibrium points around these line segments and discussed their linear stability using a control stabilization algorithm. It was later verified using Phobo's model [106]. The nonlinear stability of the equilibrium points was assessed by Arnold [107]. Further work by Riaguas and Elipe et al. found the periodic orbital families around the line segment with bifurcations, considering a non-spinning case [108]. Another simple geometry frequently used to approximate irregular small bodies is the triaxial ellipsoid [109]. Similarly, the stability criteria of the equilibrium points based on a uniformly rotating homogeneous ellipsoid model was studied in [61]. Several common features of the orbits were discovered.

Moreover, there was a lack in the analysis of the symmetry of gravitational fields.

Baoyin and Yu then studied the stability of the equilibrium points and orbits nearby asteroid 216 Kleopatra [110]. The resonant orbits near the equatorial plane of the asteroid were presented, as well as the conditions of ejected orbits [111]. Then, periodic orbital families around the asteroid were found through a scheme to search large-scale periodic orbits, showing the influence of asymmetry on periodic orbits [112].

1.4 Contents of the Thesis and Innovations

1.4.1 Contents of the Thesis

This initial chapter provides an introduction to the research status and the study of the orbital dynamics around a Solar System small body. It also discusses the motivations, objectives and innovation of the thesis.

In Chapter 2, surveys further detail into target selection and why asteroid 243 Ida was selected as the target asteroid for this study. It is then proved how the asteroid's properties are obtained either from observations, or through computational calculations. Then, detail on how to map the target SSSB's surface is presented, showing the importance of the Galileo mission. Finally, the data set utilized is demonstrated for use in later chapters.

Chapter 3 proves as an introduction to orbital dynamics, discussing the mechanical environment around small bodies and the main differences between planetary and SSSB mechanical environments. Furthermore, a general introduction to orbital dynamics around asteroids is provided, discussing which perturbations are to be taken into account and which are to be dismissed for a massless particle under the influence of a small body. The Ida-Dactyl binary asteroid system is presented, and details and hypothesis are studied. This chapter presents the initial descriptions of the gravitational field modeling for an irregular body and presents the current available methods. Advantages and limitations of each method are discussed. These methods are:

- Two-dimensional approximation

  Spherical harmonic function model

  Ellipsoid harmonic function model

- Three-dimensional approximation

  Triaxial ellipsoid model

Polyhedron model (method elected)

Particle swarm model

After, the orbital dynamics specific to each model is considered, focusing specially on the orbital dynamics for the polyhedron model, as it is the method selected to study asteroid 243 Ida. Ultimately, a general form of the orbital motion equation is presented with the potential expressed by the polyhedral method, expressing the common features of the equation form as a preliminary. A unitless form of the orbital equation is derived.

Chapter 4 focuses on developing asteroid 243 Ida's full gravity tensor for the polyhedron method. A brief introduction on the topic is provided, jumping to the mathematical approach utilized. An in-depth discussion is maintained, showing the mathematical proceeding followed. Having built the basis of the approach, the algorithm utilized is provided and the results are shown.

For Chapter 5, further hypotheses are raised so the orbital equation motions can be utilized in the vicinity of the asteroid. Moreover, equations for the gravitational and the effective potential equations are developed. Once obtained, the effective potential can be utilized to find the equilibrium points around 243 Ida. Finding the equilibrium points around asteroid 243 Ida is the ultimate goal of the study, presenting their stability. Equilibrium points are defined, and studied in detail for the the specific asteroid. Then, the stability of the equilibrium points is analyzed. A linear, rank and topological manifold classification is introduced to discuss the stability of the equilibrium points and the ressults are studied.

In Chapter 6, the limitations of the study and future directions are discussed. Large-scale periodic motion around the small body can be developed through different methods such as the Hierarchical Grid Search Method. This method searches for periodic orbits around an irregular massive body. The stability of the orbits can also be calculated through the Poincare mapping, creating a discrete system. and the topological evolution of the orbital families can be studied. Some limiting hypothesis of the polyhedron method is supposing a constant density through the asteroid and supposing a rotational velocity in a singular axis. A more complex model can be developed, were the dynamical factor is introduced.

Finally, Chapter 7 concludes the findings theorised and calculated, and develops past the initial thoughts when developing the thesis.

1.4.2 Innovations

This thesis presents asteroid 243 Ida's equilibrium points with the most precise data set available from optical imaging. Unlike prior radar observations, the accuracy of

the optical imaging provided from the "EAR-A-5-DDR-RADARSHAPE-MODELS-V1.0" data set is far superior. Therefore, there is a significant increase in faces and vertices available (16022 vertices and 32040 faces), increasing the accuracy of the results obtained. Furthermore, the polyhedron method has been applied to compute the gravitational potential of the SSSB.

Not only does it eliminate the limitations encountered with spherical harmonics (and harmonic methods in general) such as a less precise calculation, but also any arbitrary space point P can be used, regardless of whether it is inside or outside the Brillouin sphere. Finding the equilibrium points around a small body although complex, is vital for orbital dynamics and motion control of a spacecraft in the proximity of the body. Thus, allowing for spacecrafts in future missions to encounter a position (and with future work, find an orbit around these equilibrium points) that allows the spacecraft to accomplish any prospection or exploration mission. Facilitating space exploration will only benefit humankind and the development of space infrastructure, pushing research and technology further for us to understand our Universe better.

Chapter 2

Computed Properties From The Shape Of 243 Ida

2.1 Target Selection

A small percentage of all NEA with a diameter $> 200m$ have moonlets [113]. Asteroids with moonlets compose binary asteroid systems that result in complex orbital dynamics. Furthermore, most of these small bodies usually are irregular-shaped, complicating matters further. As one of the most studied binary systems within the asteroid belt, is 243 Ida-Dactyl discovered during the Galileo mission. Asteroid 243 Ida acts as the primary body while the moonlet Dactyl orbits around it, due to its relatively small size and significant mass difference. Investigating a binary system allows for huge advancements in the study of dynamic orbital characteristics. Furthermore, the Galileo mission was the first spacecraft to orbit an exterior planet of the Solar System. Moreover, it was the first mission to return imaging and complete a flyby of an asteroid, opening wide research interest in other asteroids and orbital dynamics around small bodies. Among other interesting findings were the liquid water ocean under the icy surface of Europa, Jupiter's moon [11], as well as being the first spacecraft to operate in Jupiter's magnetosphere, identifying its global structure.

The evolution of the geologic features from a small body is complex and involves abundant dynamical phenomenons that affect its orbital behaviors. For instance, asteroids take many micro-meteorite impacts [92], leaving a trace in the form of a crater for a prolonged extension of time [93]. From the asteroid's ejecta, some will be able to escape the asteroids vicinity, while other will be trapped in a temporary orbit around the asteroid [94], leaving the rest to fall back to the surface and re-accumulate. Investigating the 243 Ida-1 Dactyl binary system facilitates understanding the physical formations found as the principal asteroid's surface.

2.2 243 Ida

The asteroid finds itself as the fourth largest of the Koronis family, with an estimated size of $59.8 \times 25.4 \times 18.6km$ [114]. Other important physical parameters such as its mass is estimated to be $4.2 \pm 0.6 \times 10^{16}kg$ [115]. Dactyl's mean radius is $\sim 0.7km$, having an oblate shape, with its 3 axes of length $1.6 \times 1.4 \times 1.2km$ [116]. Asteroid 243 Ida's density was estimated to be $2.6gcm^{-3}$, with an uncertainty of $\pm 0.5gcm^{-3}$ [117]. Its rotational period was calculated to be $4.633632h$ [118]. The most precise shape model of asteroid 243 Ida includes *16022* vertices and is an improvement from the prior model that included 5040 vertices [119].

As ground observations are very limited, the Galileo spacecraft executed and obtained data from the solid state imaging (SSI) experiment at the encounter of various asteroids. Galileo first encountered Gaspra. Its second asteroid encounter occurred on the final leg of the VEEGA trajectory to Jupiter. On August 28, 1993, at 16:52:04.7 UTC [120], the Galileo spacecraft visited 243 Ida. While 951 Gaspra is an olivine rich S-type asteroid [121], the near-infrared spectrum of 243 Ida is more typical of S-type asteroids with a higher propensity to have pyroxene [122].

The solid state imaging experiment for Ida had three objectives:

- Fully characterize shape and rotation state.
- Obtain images with highest possible spatial resolution at high solar incidence angle for the investigation of geologic and evolutionary processes.
- Obtain color and photometrically calibrated images for the investigation of microphysical and compositional properties of surface materials.

Even though the SSI objectives were similar to those for Gaspra, the successful experience led to a goal of increased performance. Therefore, the sequence at Ida included a high-risk pointing and mosaicking strategy to obtain images with a spatial resolution of approximately 25 meters per pixel at the time of closest approach.

Finally, Stooke developed the following data set: EAR-A-5-DDR-RADARSHAPE-MODELS-V1.0 [119] Further explanations of the data set is to be found in Chapter 4. With the data set, all surface points could be mapped and a visual representation was to be obtained as seen in Fig. 2.1

Simultaneously, two topographic maps are computed from the geometric data acquired, representing both the distance of each surface point of asteroid 243 Ida to the center of mass, and the heights at which the surface lies. These maps have been computed and represented in Fig. 2.2 respectively.

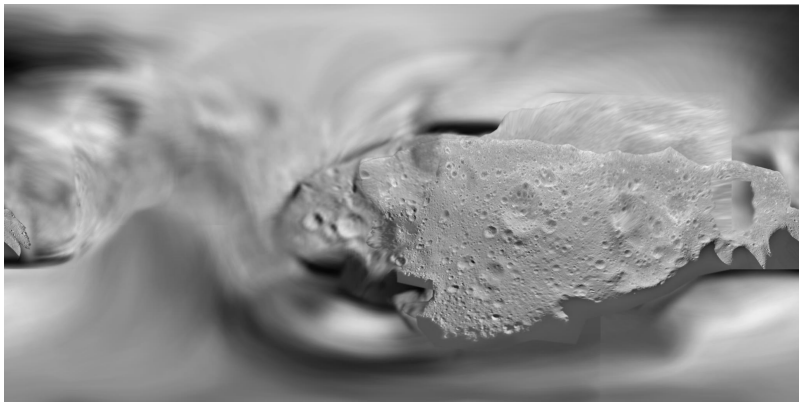

Figure 2.1: Mosaic of asteroid 243 Ida. [119]

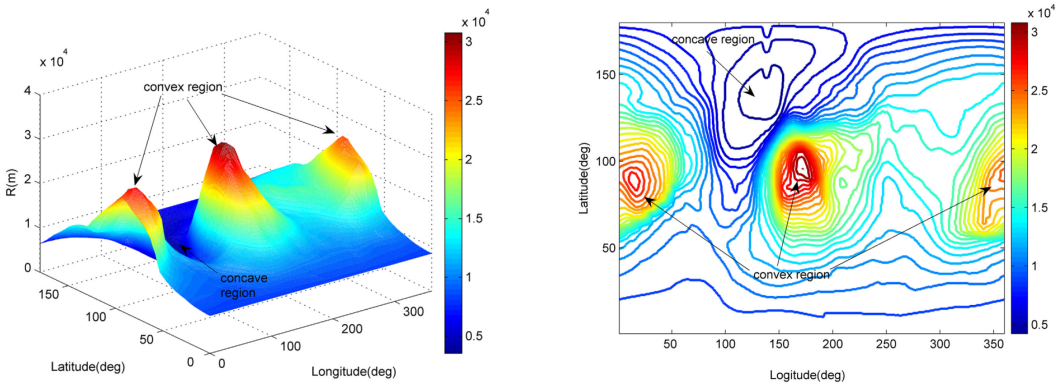

(a) Topographic map denoting the distance to the center of mass of asteroid 243 Ida.

(b) Topographic map denoting the height of the surface of asteroid 243 Ida.

Figure 2.2: Topographic maps of asteroid 243 Ida.

Chapter 3

Modeling Orbital Dynamics in the Potential of Solar System Small Bodies

3.1 Mechanical Environment In The Vicinity of Small Bodies

3.1.1 General Introduction To Orbital Dynamics Around Asteroids

Approximately 90% of known small bodies are to be found at the main asteroid belt between the orbits of the planets Mars and Jupiter, at roughly 2.17-3.64 AU away from the Sun. A major part of the remaining 10% belong to the near-Earth objects (NEO's) which are a potential hazard to the Earth. Observing plans like Near-Earth Asteroid Tracking (NEAT) and Lincoln Near-Earth Asteroid Research (LINEAR) monitor these small bodies for long terms [123]. Research nowadays classifies the asteroids according to their orbital features into three categories: Amor asteroids, with an orbit that approaches that of Earth's but does not cross; Apollo asteroids, whose orbits cross Earth's orbit, within Mars' orbit, and some with high eccentricities; Aten asteroids, with an orbit that crosses that of Earth's, but unlike Apollos, spend most of their time inside Earth orbit.

There is a gigantic number of Solar System small bodies (SSSB), and their orbits are diverse. To this date, we lack knowledge about the real spatial environment around SSSB. Many known perturbations may affect SSSB, but only a few have a significant effect on the short-term motion of a spacecraft. Among these are, the gravitational perturbations from the Sun and planets, the solar radiation pressure, dust from meteorite impacts and collisions from ejected debris, and the Yarkovsky effect which is a force that acts on a rotational body in space due to an anisotropic

emission of thermal photons that carry momentum. The effect of dust has proven to be too complex for this study, due to its randomness and uncertainty, whereas the Yarkovsky effect is usually considered for small asteroids of diameters up to $\approx 10km$. Asteroid 243 Ida has a far superior diameter, therefore its effect is neglected in this study. More general perturbation forms are considered, like solar radiation pressure and the third-body gravitational perturbation.

3.1.2 Perturbations And What To Dismiss

Planetary gravity has been researched since 1866, when Kirkwood (American astronomer) found the narrow gaps in the distribution of the semi-major axis of the orbits of the main-belt asteroids. Nowadays, the gap is known as Kirkwood Gap [124]. Orbital resonances with Jupiter resulted in these gaps, at specific orbital distances that resulted in simple ratios with the planet. The gaps occur at the 2:1, 3:1, 5:2 and 7:3 orbital resonances.

The acceleration of a mass point orbiting around a small body can be represented as

$$\frac{d^2}{dt^2}\mathbf{r} \approx \mathbf{a} + \mathbf{a_s} + \mathbf{a}_\odot, \tag{3.1}$$

where r is the position vector of the mass point, $\mathbf{a}$, indicates the gravitational acceleration from the small body, $\mathbf{a_s}$, is the acceleration due to the solar radiation pressure, and $\mathbf{a}_\odot$ is the solar tidal acceleration. As the equation proves, there are two main forms of perturbations: solar tide and solar radiation pressure. To check if any can be neglected, the order of magnitudes of the perturbations must be analyzed. The definition of the influential sphere of a small body is presented.

$$R = D\left(\frac{M_A}{M_\odot}\right)^\alpha, \tag{3.2}$$

in which, M_A and $M_\odot$ are the masses of the small body and the Sun respectively, D is the mean distance from the small body to the Sun. For 243 Ida, D is equal to 2.862 AU. The exponent parameter α is responsible for discriminating the boundaries of these spherical regions. There are three common ways to define the radius R, as a function of the exponent parameter α: $\alpha = 1/3$ corresponds to R_1, meaning that the magnitude of the solar tide is equal to the small body's gravity at the boundary, as is defined by a Hill Sphere; $\alpha = 2/5$ corresponds to R_2, is the classical definition of Sphere of Influence used in astrodynamics and describes the boundary of the region in which the dominant gravity on an orbiting object (e.g. satellite) is from the small body; $\alpha = 1/2$ corresponds to R_3, meaning that the magnitude of the solar gravity equals that from the small body at the boundary.

According to the different definitions of the radius, $R_1 > R_2 > R_3$. Using the latest

R	R_1	R_2	R_3
α	1/3	2/5	1/2

Table 3.1: Definition of radius of influential sphere and its corresponding α values.

mass information, 243 Ida's radii can be calculated:

Asteroid	$M_A/M_\odot$	$R_1(km)$	$R_2(km)$	$R_3(km)$
243 Ida	2.20×10^{-14}	8.32×10^3	1.47×10^3	6.35×10^1

Table 3.2: Values of the influential sphere radii specific to 243 Ida.

Yang et al. describes the values of the three radii obtained from Eqn. 3.2 for 23 different asteroids and found that the scaled mass of known small bodies, M_A/M_S, ranges from 5.03×10^{-21} to 4.74×10^{-10}. The following table shows the values calculated.

Asteroid	$M_A/M_\odot$	$R_1(km)$	$R_2(km)$	$R_3(km)$
1 Ceres	4.81×10^{-10}	2.25×10^5	7.77×10^4	9.09×10^3
2 Pallas	1.00×10^{-10}	1.33×10^5	4.15×10^4	4.15×10^3
4 Vesta	1.38×10^{-10}	1.27×10^5	4.02×10^4	4.15×10^3
10 Hygiea	5.60×10^{-10}	1.25×10^5	3.72×10^4	3.51×10^3
11 Parthenope	2.56×10^{-12}	3.48×10^4	8.47×10^3	5.87×10^2
15 Eunomia	1.20×10^{-11}	6.27×10^4	1.69×10^4	1.37×10^3
16 Psyche	9.00×10^{-12}	6.30×10^4	1.67×10^4	1.31×10^3
20 Massalia	2.44×10^{-12}	3.36×10^4	8.16×10^3	5.63×10^2
45 Eugenia	3.00×10^{-12}	4.07×10^4	1.00×10^4	7.05×10^2
52 Europa	2.60×10^{-11}	9.52×10^4	2.70×10^4	2.36×10^3
87 Sylvia	7.60×10^{-12}	7.13×10^4	1.87×10^4	1.44×10^3
88 Thisbe	7.00×10^{-12}	5.49×10^4	1.43×10^4	1.10×10^3
90 Antiope	4.14×10^{-13}	2.44×10^4	5.27×10^3	3.04×10^2
121 Hermione	4.70×10^{-12}	5.99×10^4	1.52×10^4	1.12×10^3
216 Kleopatra	2.33×10^{-12}	1.98×10^4	3.33×10^3	2.28×10^3
243 Ida	2.20×10^{-14}	8.32×10^3	1.47×10^3	6.35×10^1
253 Mathilde	5.19×10^{-14}	1.02×10^4	1.92×10^3	9.02×10^1
433 Eros	3.60×10^{-15}	2.32×10^3	3.64×10^2	1.31×10^1
444 Gyptis	4.00×10^{-12}	4.56×10^4	1.14×10^4	8.29×10^2
511 Davida	5.60×10^{-11}	1.26×10^5	3.75×10^4	3.54×10^3
704 Interamnia	3.50×10^{-11}	1.04×10^5	3.01×10^4	2.71×10^3
762 Pulcova	1.28×10^{-12}	3.56×10^4	8.26×10^3	5.34×10^2
766391 1999KW4	1.10×10^{-18}	6.88×10^1	6.30×10^0	1.01×10^{-1}

Table 3.3: Values of the influential sphere radii of the 23 asteroids.

As demonstrated in the table, the maximum radius R_1 usually is hundreds of times bigger than the size of the asteroid, while the minimum radius R_3 is only tens of times, which represents a strict estimation of the dominated range by the small body.

Hamilton et al. study suggested that the Hill radius can be used to estimate the region where a satellite might exist, after studying the orbital stability of natural satellites of the small bodies, i.e., the asteroid's gravity dominates the orbital motion within this region [97]. To study the effect of the solar radiation pressure and tides at the boundaries of the spherical regions, we develop the following dimensionless equations, scaled by the asteroid gravity. When combined with prior equation Eqn. 3.2, the scaled perturbations depend on the mass ratio of the small body and the Sun like:

$$a_s/a \approx \beta \frac{GM_\odot}{D^2} / \frac{GM_A}{R^2} = \beta \left(\frac{M_A}{M_\odot} \right)^{2\alpha-1}, \tag{3.3}$$

$$a_\odot/a \approx \frac{R}{D} \frac{GM_\odot}{D^2} / \frac{GM_A}{R^2} = \beta \left(\frac{M_A}{M_\odot} \right)^{3\alpha-1}. \tag{3.4}$$

Where $a_\odot$, a_s, a indicate the magnitudes of $\mathbf{a}_\odot$, $\mathbf{a_s}$, $\mathbf{a}$, respectively. β is the ratio of the radiation pressure force to the gravitational force of the Sun. For this analysis, applying the general magnitude of β for a spacecraft is sufficient. According to [125], $\beta = 3.37 \times 10^{-4}$.

Fig. 3.1 has been graphed to make sense of the variation of the perturbations with the mass using three typical asteroids, including Vesta $\sim 525.4km$, Eros $\sim 16.8km$ and 1999KW4 $\sim 1.4km$. The three asteroids have been chosen as they represent almost completely the entire spectrum of mass ratios. It can be seen in Fig. 3.1, the magnitudes of the scaled solar radiation pressure **(a)** and solar tide **(b)** are plotted over this range at R_1, R_2 and R_3 respectively. A value over 10^0 indicates the perturbation is greater than the effect of gravity, whereas if it is below 10^0 will indicate that the perturbation is small enough compared to gravity to be neglected.

Fig. 3.1 reflects how both solar tide and solar radiation pressure cannot be neglected for the study of orbital motion beyond R_1, when the latter is greater than the gravity, and the latter is equivalent with the gravity. At a distance of R_2, solar tide can be neglected while the effect of solar radiation pressure will depend on the mass of the small body; being considerable for small objects like Eros, and ignorable for bigger ones like Vesta. For a distance of R_3, both solar perturbations are smaller than the gravity, being the solar tide smaller than that of solar radiation pressure. Hence, can be confirmed that the gravity of a small body is the dominant force governing

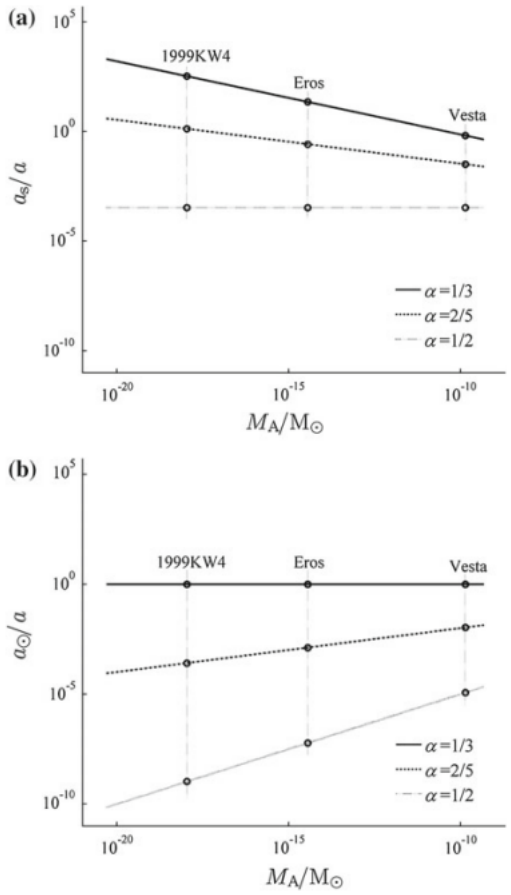

Figure 3.1: Perturbations scaled as a function of a varying mass of the SSSB. (a) Solar Radiation Pressure. (b) Solar Tide.

the motion within the spherical region of radius R_3, which will usually be tens of times that of the small body's diameter, meaning the solar tide and solar radiation pressure perturbations are negligible when studying the short-term orbital motion of a spacecraft around a small body.

3.1.3 243 Ida

16% of all near-Earth asteroids with diameters greater than $200m$ have moonlets [113], representing complex asteroid systems composed of highly irregular-shaped bodies that result in extremely complex dynamic orbital characteristics. 243 Ida-Dactyl is a commonly investigated binary asteroid system from the asteroid belt between Mars and Jupiter. It consists of a relatively small moonlet body (Dactyl) orbiting a much larger primary body (Ida). It belongs to the family of asteroids Koronis whose origin is supposed to be the result of the collision of two major bodies [114]. Dactyl was discovered by the Galileo spacecraft during its approach to the asteroid [11] - [13].

The asteroid finds itself as the fourth largest of the Koronis family, with an estimated size of $59.8 \times 25.4 \times 18.6km$ [114]. Other important physical parameters such as its mass is estimated to be $4.2 \pm 0.6 \times 10^{16}kg$ [115]. Dactyl's mean radius is $\sim 0.7km$,

having an oblate shape, with its 3 axes of length $1.6 \times 1.4 \times 1.2km$ [116]. Asteroid 243 Ida's density was estimated to be $2.6gcm^{-3}$, with an uncertainty of $\pm 0.5gcm^{-3}$ [117]. Its rotational period was calculated to be $4.633632h$ [118]. The most precise shape model of asteroid 243 Ida includes *16022* vertices and is an improvement from the prior model that included 5040 vertices [119].

The origin of a binary asteroid system can derive from the rotational breakup of asteroids [126]. Evermore, the Yarkovsky-O'Keefe-Radzievskii-Paddack (YORP) effect may increase an asteroid's spin rate, leading to its internal material structure failure, resulting in further rotational breakup [127]. Another method to generate multiple asteroid systems is by meteorite impacts [128]. This will inevitably lead to an endless variety of shapes. Landslides and mass shedding on asteroid surfaces may also vary its shape over time [129, 130].

Rocco et al. considered an orbital motion of a spacecraft around Ida, perturbed by the gravitational attraction of Dactyl [131]. The moonlet's orbit is almost circular with a radius of $90km$, mass of $2380kg$, and non-central gravitational field of Ida [132]. Study concluded that the main disturbance in the trajectory of the spacecraft was due to the gravitational potential of Ida. The disturbance caused by Dactyl is insignificant since the estimated mass of the natural satellite is very small, and its orbit was not adequately determined and varies due to the gravitational perturbation of Ida.

Therefore, the gravitational field of Ida must be precisely mapped for an accurate study of the dynamic environment around the asteroid so that a satellite trajectory can be calculated.

3.2 Descriptions Of The Gravitational Field

3.2.1 Introduction

Gravitational field modeling is one of the main building blocks required for analyzing orbital motion characteristics. There are great challenges due to the variety of shapes present in small celestial bodies. The two commonly employed methods for gravitational field modeling are: series approximation and three-dimensional approximation. On one hand, series approximation methods usually approximate the gravitational potential energy by utilizing special functions such as spherical and ellipsoidal harmonic functions. On the other hand, three-dimensional approximation generally approximates the gravitational potential energy by modeling simplified geometrical bodies, in the likes of triaxial ellipsoid, polyhedral, and particle swarm model.

3.2.2 Series approximation

Spherical harmonic function model

In his 1807 *"Memoire sur la propagation de la chaleur dans les corps solides"*, Jean-Baptiste Joseph Fourier presented what would later be known as Fourier series, due to his important contributions to the study of trigonometric series. Later in the 19th century, the method by Fourier series to approximate gravitational potential function had been proposed. This method proved to be complex and had a slow convergence rate, so the method did not win popularity. Meanwhile, Legendre's polynomial function for the series approximation was proposed in 1936. This method provided a much higher rate of convergence, becoming widely used in gravitational field modeling of Earth, Mars, and other planets. In the late 20th century, the spherical harmonic model theory was elaborated. This new model presented advantages, such as simplicity, small computation power required, an explicit analytic expression of gravitational potential energy and readily derived coefficients. The coefficients of the harmonic function can be achieved based on in-orbit data. The analytical solution has been derived to describe perturbed orbital motion, summarizing the influence of non-spherical gravitational field on probe orbit. Due to its advantages, the spherical harmonic function model is widely employed in the research of orbital dynamics and celestial mechanics.

Nonetheless, the spherical harmonic model proves some drawbacks, resulting in analysis errors of the motion. These can be summed into two main points: convergence domain problem and truncation error. To approximate the gravitational potential energy, one should theoretically use infinite series. However, only finite terms can be calculated when computed. This will inevitably lead to error, making calculated results differ from the ideal. Rossi et al. [133] studied the truncation error and found that as distance between sample points and small bodies shortened, it became more significant. This will lead to a severe error during the gravitational field modeling. Meanwhile, the convergence domain problem (based on Legendre polynomials) means that the spherical harmonics function could only take effect outside the Brillouin sphere. For planets and particular small bodies like 1 Vesta (due to its planetoid-like size), the function has no remarkable influence on gravitational field modeling. However, most small celestial bodies of interest in our Solar System are irregularly shaped meaning that most regions may be located within the Brillouin sphere, so the influence of convergence becomes apparent, as shown in Fig. 3.2.

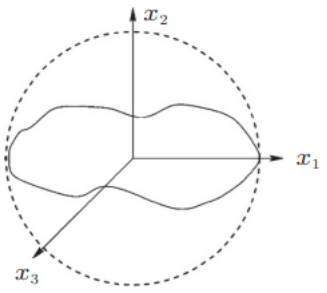

Figure 3.2: Brillouin Sphere of a SSSB.

Once the probe is located within the Brillouin sphere, independently of how many orders of the spherical harmonic expansion can be preserved, the gravitational potential function cannot be accurately approximated. This will incur difficulties for any activity as of the following: flying around the small celestial body at close range; control and design of trajectory; orbital dynamics analysis of hovering and landing. To solve the problem, the ellipsoidal harmonic model was developed.

Ellipsoid harmonic function model

Instead of employing Legendre polynomials, Hobson [2] proposed in the middle of the 20th century an ellipsoidal harmonic model applying the Lamé polynomial approximation [134]. This model will provide a better description for irregular-shaped bodies by ellipsoidal harmonic coefficients, helping to construct the gravitational field [134, 135]. Later, Pick et al. established the ellipsoidal harmonic function theory in 1973 [136]. When compared to the spherical harmonic function model, the ellipsoidal harmonic model extends convergence domain much closer to the small body's surface. The Brillouin ellipsoid for a generic small celestial body can be appreciated in Fig. 3.3.

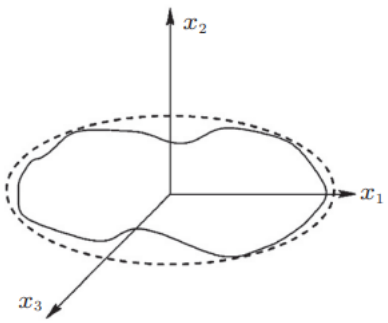

Figure 3.3: Brillouin Ellipsoid of a SSSB.

As is shown, the region near the small body's surface can be more precisely approximated by the Brillouin ellipsoid. This method will effectively solve the spherical harmonic model's convergence problem near small celestial body surfaces. It has been employed by Garmier and Barriot to design the landing orbits around Wirtanen comet and implemented a series of simulation experiments [58]. With the results of the analysis, they proved that the ellipsoid harmonic model may be used in designing landing orbits. Nevertheless, the model has disadvantages such as long CPU time, complex algorithm, and complicated derivation of harmonic coefficients. Dechambre and Scheeres developed a method to simplify the algorithm by converting the ellipsoidal harmonic coefficients to spherical [137]. This simplifies the solution of the ellipsoidal harmonic coefficients and built a solid foundation for the promotion and application of this method.

3.2.3 Three-dimensional approximation

Triaxial ellipsoid model

The triaxial ellipsoid model is the most common and typical method in three-dimensional approximation. It relies on approximating the shape of a small body

by using a triaxial ellipsoid, from which the gravitational potential function can be obtained by integrating the triaxial ellipsoid body. The three major-axes of the ellipsoid model are the length, width, and height. The model is represented in Fig. 3.4.

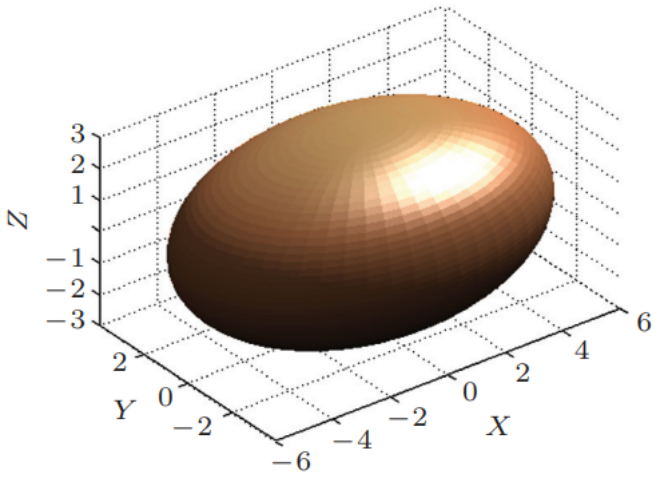

Figure 3.4: Triaxial Ellipsoid model of a SSSB.

The method provides with three clear advantages: data easily obtained by astronomical observation, small amount of calculation and a more fitting representation of the gravitational field, as it usually resembles the irregular shape of the asteroid more precisely. Nonetheless, as it occurs with the ellipsoid model, this method also inevitably leads to error during the research due to variable shapes.

Polyhedron model

To obtain precise gravitation field, the polyhedron model is employed. In general, the polyhedral model and the particle swarm model approximate an irregular-shaped asteroid through new geometrical bodies. By line and area integrals, the gravitational potential energy is derived to represent the gravitational field of the small celestial body. The polyhedral model is proposed by Werner [138], and then developed into a relatively comprehensive method theorized by [136], and used by [139].

As it will later be discussed, this will be the method utilized to represent asteroid 243 Ida. The asteroid can be visualized in Fig. 3.5.

Particle swarm model

Next to the polyhedron model, it is one of the two classical paradigms employed to obtain precise gravitational field. The particle swarm method usually applies cubes or micro-spheres with differing densities to approximate irregular-shaped small bodies, making it a more precise model than the former methods exposed.

Foregoing analysis proves that two typical methods (series and three-dimensional

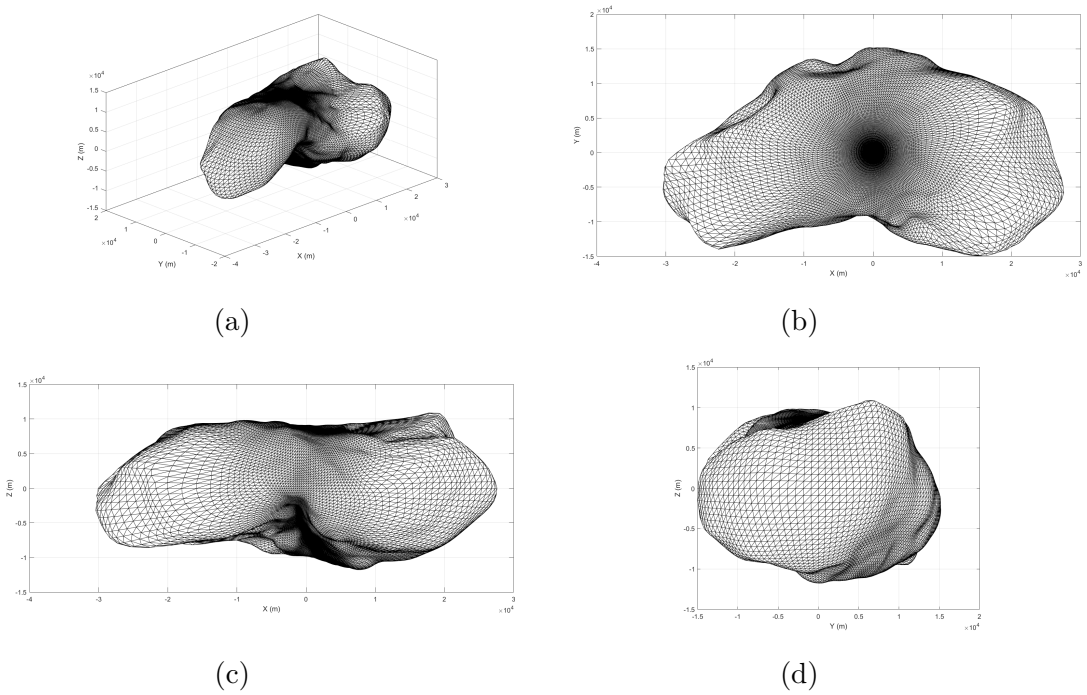

(a) (b)

(c) (d)

Figure 3.5: Polyhedral model of asteroid 243 Ida from different perspectives - (a) 3D View. (b) xy Plane. (c) xz Plane. (d) yz Plane.

approximation) both carry advantages and drawbacks. On one hand, spherical harmonic or ellipsoidal harmonic function provide relevant analytical expressions and description of motion behavior. This facilitates quantitative and qualitative theoretical analysis but fails to develop a highly precise gravitational field. On the other hand, triaxial ellipsoid, polyhedron and particle swarm models derive a highly precise gravitational field but fail to provide an analytical expression of the potential energy function.

3.2.4 Orbital dynamics of small celestial bodies

Various motional behaviors can be classified when studying the orbital dynamics around small celestial bodies. Motional characteristics will be influenced mainly by spin, shape, and other physical parameters. According to controlled condition of motion around small celestial body, the orbit may be classified into one of two categories: natural and controlled motion. Natural motion is an orbital motion only affected by the gravitational force of the small body, non-spherical perturbation force, and any other natural forces. Controlled motion forms under the combined effects of natural and controlled forces.

The natural motional orbit is distinguished into orbiting around the center or around the equilibrium point.

Orbital dynamics of small celestial bodies

There may exist surrounding orbits like that observed of a planet when small celestial bodies have large masses, but its motional behavior will differ vastly. Orbital

energy and angular momentum of a probe may greatly change due to the spin effect and non-spherical perturbations of a small celestial body. Therefore, the existence and study of the stability of the orbit is the major issue of orbital dynamics. Corresponding to the gravitational field model used, these researches are classified into three categories:

- The orbital dynamics based on spherical harmonic or ellipsoidal harmonic models.
- The orbital dynamics based on triaxial ellipsoid models.
- The orbital dynamics based on polyhedral models.

Orbital dynamics based on spherical harmonic or ellipsoidal harmonic model of small bodies

Scheeres and Hu [9-11] carried a great amount of research based on spherical and ellipsoidal harmonics, considering the second degree and order gravity field as a typical model of the gravitational field [69, 95, 70]. Firstly, the second degree and order gravity field with no rotation are used for motional types and qualitative analysis. Secondly, results demonstrated that the motional plane of a particle around the small celestial body will precess or be fixed along the minimum or maximum moment of inertia of the body. After that, the particle's motion problem was investigated in a slow-rotation gravitational field. The relational average Lagrange planetary equations were derived. To develop the motional description of the particle, the Lagrange planetary equations are combined with the Jacobi integral. Studies proved that slow rotation leads to a 1:1 resonance of the orbital plane with the rotating body, with a critical value. If spin speed is greater than the critical value, then the motion due to resonance stops. [70].

Scheeres and Hu [12,13] proposed the assumption of a homogeneous spin to derive the criterion of the second degree and order gravity field [70, 140]. Applying the criterion, stability of near circular equatorial orbits was evaluated. Regions of stable and unstable motion were presented, leading to the discussion of the equilibrium points and orbital families that exist. The stability of the orbital families was investigated for different spin-rates [140].

The research undergone provides an insightful and clear bases of the motional characteristics in the second degree and order of gravity fields. Hu et al. researched the preliminary motion around a small celestial body, analyzing the influence of a dynamical environment [141]. Using Castalia asteroid as an example and taking the second degree and order gravity field, the investigation obtained the characteristics of control and dynamics around small celestial bodies.

Orbital dynamics around small bodies based on triaxial ellipsoid models

In astronomical observation, the triaxial ellipsoid model is the common method to use. There are few researches based on this model but are sufficiently representative. Scheeres was the first to investigate the orbital dynamics with spin, in the triaxial homogeneous ellipsoid gravity [61]. Spin rate and shape of the small celestial body will determine how it classifies into one of the two existing categories. It was found that any synchronous orbit within any of these categories are unstable, and that the stability of a quasi-synchronous orbit will depend on the types of triaxial ellipsoid bodies. Using 1 Vesta and 433 Eros as examples, research validated these conclusions [61]. Later, Cui et al. studied a possible motion around asteroids by using triaxial ellipsoid bodies [142]. This investigation showed the zero-velocity curve, analyzed a possible area of motion for the probe and proposed boundary conditions of collision between the probe and the asteroid. After that, investigation proved the effect of an asteroid's oblateness and ellipticity on the orbital perturbation, especially for slow-spin asteroids. Some frozen orbital families and their stability were presented. Cui et al. used the previous investigation for Ivar asteroid [142]. The zero-velocity curve and collision boundary conditions were determined, and the effect of the oblateness and ellipticity of the asteroid on the orbit was also analysed [143]. In 2007, Byram used the triaxial ellipsoid model for the gravitational field of comet nuclear and analysed the orbital dynamics of a probe near the comet. Meanwhile, proposing a coma conical jet model and investigating the damping effect of the comet shape and gas, on the orbit of the probe [144].

In conclusion, it is shown that the research framework of the triaxial ellipsoid model for orbital dynamics has been established. The triaxial ellipsoid models have been classified, specific type of orbits and relationship with stability have been found, and motion near small celestial bodies and comets have been investigated. Further studies on motion characteristics of orbits are required in the near future, studying the existence of periodic and quasi-periodic orbits and their stability.

Orbital dynamics of small celestial body based on precise polyhedron models

Up until this day, the polyhedral model and the particle swarm model have proved to be the most accurate models for gravity fields of small celestial bodies. As more research is undertaken, improvements lead to more mature and accurate developments of the models.

Scheeres et al. used asteroid 4769 Castalia asteroid as example to study its orbital dynamics based on the polyhedral model [68]. Research proved the existence of periodic orbits around the asteroid. Further analysis showed that all direct and synchronous orbits in the region with triple average diameter of the asteroid, are unstable and prone to either collide with the asteroid or escape it. Conditions and the regions of capture and escape were calculated through numerical analysis [68]. The research also provided with the basic laws of motion near the asteroid, laying a strong foundation for future close exploration of asteroid 4769 Castalia.

Another asteroid that received attention was asteroid 4179 Toutatis. The asteroid was Chang'E-2 (CE-2) probe's target. Later, Scheeres et al. presented the polyhedral model for asteroid 4179 Toutatis and studied its orbital dynamics [69]. The research proved that it is a Hamiltonian system and therefore, possesses all its properties. Nevertheless, there is no Jacobi constant, and the zero-velocity surface cannot be used to determine its motional behavior. Using the Lagrange equations of planetary motion, the so called "frozen orbits" (quasi-periodic) were found. Some of the orbits were found to be stable, especially the retrograde family. Asteroid 4179 Toutatis is a typical self-spin, non-spindle asteroid. The research determined the orbital dynamics specifically for Toutatis, but is yet to determine if all non-spindle spin asteroid share the same properties found.

The stability of periodic orbits has been investigated in more detail lately. Yu and Baoyin employed the polyhedral model of asteroid 216 Kleopatra asteroid to study the dynamic behavior and stability of three-dimensional periodic orbits [112, 111]. The research found 29 basic periodic orbit families, and the stability evolution and motional characteristics were determined. Resonance orbit families near Kleopatra were also investigated. Lara and Scheeres studied through numerical analysis the boundary conditions of stability of three-dimensional orbits around a small celestial body [81]. Furthermore, the investigation analyzed orbital stability of three-dimensional periodic orbits and discussed the resonance orbits. Additionally, other researchers have proposed terminator orbits, [29] as they present strong robustness under all kinds of perturbation forces, such as solar radiation pressure force, weak gravity force, non-spherical perturbation force, and so on [145]. These orbits satisfy almost completely the requirements for long time in-orbit work [69, 83].

The trend in the research of orbital dynamics has been to investigate periodic orbits, frozen orbits, terminator orbits, and stability issues. Due to variable spin, shape, and other physical parameters, these topics have proven to be very challenging.

3.3 Motion Equations

The motion equations of a test mass point in the vicinity of a small body are given in Chapter 5. As a brief introduction, the general orbital motion equation is presented, but will later be discussed in further detail.

Considering a massless point, meaning that the mass point does not exert any gravitational influence on the small body, the motion equation will be:

$$\frac{d^2}{dt^2}\mathbf{r} \;=\; -\nabla U. \tag{3.5}$$

If the left side of the equation is expanded, the orbital motion equation will look like this

$$\ddot{\mathbf{r}} \; + \; 2\omega \times \dot{\mathbf{r}} \; + \; \omega \times (\omega \times \mathbf{r}) \; + \; \alpha \times \mathbf{r} \; + \; \frac{\partial U(\mathbf{r})}{\partial \mathbf{r}} \; = \; 0, \tag{3.6}$$

where ω and α are denoted as the small body's angular velocity and acceleration respectively. Further development of the equation is later completed.

Chapter 4

Full Gravity Tensor of the Polyhedral Model

4.1 Introduction

To obtain the full gravity tensor of the asteroid it has been concluded that the best method to use is the polyhedral model. The gravitational signal from a polyhedral source has been thoroughly studied, both analytically and numerically. The former provides an exact solution, while the latter provides an approximate solution. Among the plentiful contributions for the closed analytical solution, most authors revolve their work around the gravitational attraction; the gradient of the gravitational potential induced by a polyhedral source. Meanwhile, they do not use a uniform triangulation of the polyhedron. In 1976, Barnett developed a closed analytical expression of the gravitational attraction of a polyhedral source by applying a triangular mesh, representing its outer boundary surface [53]. Later, Pohanka provided an analytical expression using a more general triangulation [66]. Other contributions for the analytical solution of the gravitational potential and the gradient of the gravitational potential of a general polyhedron include [146, 147, 148, 149, 150, 151, 152, 138, 153].

In 1979, Okabe presents for the first time, an algorithm for the first and second-order derivatives from an arbitrary polyhedron [154]. Okabe omitted singularities the algorithm could encounter. Later, Werner and Scheeres completed the analytical scheme of Werner from 1994 [138] , by developing the expressions for the gravity gradient tensor and applying them to problems of dynamic astronomy [63]. Meanwhile, Petrovic also derived a closed expression for the full gravity tensor basing it on the application of Gauss' divergence theorem twice: firstly, for the transition from volume to surface integrals, and secondly for the transition to line integrals along the closed polygons defining each polyhedral face [65]. The tensor contains the potential, first-order derivatives, and the complete tensor of the second-order

derivative. In 2001, Tsoulis and Petrovic [15] refined the mathematical approach, presenting the derivation of certain singularity terms. The refinement overcomes the singularities, allowing the line integral formalism to be applied everywhere in space.

Finally, Tsoulis comprehensively provided the methodology and an accompanying computer program for the line integral approach [67]. The clarity and geometric insight of the algorithm make it easily accessible and points out the algorithmic details of the formalism, due to the occurrence of the singularities. Therefore, the algorithm proves to be beneficial to different applications. Astronomy and more specifically, developing a small irregular celestial body, is one of them.

4.2 Mathematical Approach

4.2.1 The Line Integral Approach

When considering a polyhedral solid of finite number of planar faces that meet along segments, a general polyhedron implies that the number of segments of each face in the polygonal shape, may differ between faces. Vertices are defined at the two ends of each segment. An assumption that the including mass has a constant density must be made to develop the general expressions for the gravity field for the polyhedral method. Previous implementations of a constant density assumption were utilized using mascon models, as they were an improvement to spherical harmonics [155]. The polyhedral mass is evaluated from an arbitrary space point P.

$$U \;=\; G\rho \int\int\int_V \frac{1}{l} dV, \tag{4.1}$$

$$U_{x_i} \;=\; G\rho \int\int\int_V \frac{\partial}{\partial x_i}\left(\frac{1}{l}\right) dV, \;\; (i = 1, 2, 3), \tag{4.2}$$

$$U_{x_i x_j} \;=\; G\rho \int\int\int_V \frac{\partial^2}{\partial x_i \partial x_j}\left(\frac{1}{l}\right) dV, \;\; (i, j = 1, 2, 3) \tag{4.3}$$

Where V indicates the volume, G the gravitational constant taken equal to $6.67259 \times 10^{-11} m^3 kg^{-1} s^{-2}$ and ρ as the constant density of the polyhedral distribution taken as $2670 kgm^{-3}$.

Furthermore, the distance function can be defined to refer the space point P to a coordinate system with origin ($x_1^{'} = x_2^{'} = x_3^{'} = 0$) and basis of orthonormal unit vectors ($\mathbf{e_1}, \mathbf{e_2}, \mathbf{e_3}$) at P.

$$l \;=\; \sqrt{(x_1 - x_1')^2 + (x_2 - x_2')^2 + (x_3 - x_3')^2}, \tag{4.4}$$

Eqn. 4.1 conveys the gravitational potential. The three expressions from Eqn. 4.1 - 4.3 expresses the three components of the gravitational attraction vector with respect to the coordinated system aforementioned, where i indicates the partial derivative components according to $U_{x_i} = \left(\frac{\partial U}{\partial x_i}\right), i = 1, 2, 3$. Eqn. 4.3 describes the nine elements of the tensor of the second order derivatives according to $U_{x_i x_j} = \left(\frac{\partial^2 U}{\partial x_i \partial x_j}\right), i, j = 1, 2, 3$. Nevertheless, as the tensor has symmetry and due to the validity of Laplace's equation for the terms in the tensor's diagonal, only five of the elements are unknown. This leaves the three equations with nine unknown terms.

The integrals from the three equations are transformed applying the divergence theorem of Gauss. The final expressions are independent of the coordinate system chosen during the transformation. The transformation occurs in two stages. Initially, the volume integrals are transformed into surface integrals by applying Gauss' divergence theorem. The number of surface integrals obtained is equal to the number of faces of the polyhedral shape. It expresses the projection of the computation point P onto each face of the polyhedron. Assuming the polyhedron consists of n faces, n projections of the point P as $P_i^{'}$ will be obtained, where $i = 1, \ldots, n$. Then, the divergence theorem is applied once more on the plane of each face, transforming each surface integral into a set of line integral defined for each segment belonging on that face. Thus, projecting the n $P_i^{'}$ values onto each line segment j of the face. Assuming there is m segments in total per face, the transformation produces $n \times m$ points $P_{ij}^{'}$, where $i = 1, \ldots, n$, $j = 1, \ldots, m$, with m possibly varying between faces. Final expressions contain a double summation of certain functions defined over each segment, for the given number of faces and segments, with a total of $n \cdot m$ line integrals.

The application of Gauss theorem to the three equations equals the retrieval of three vector fields, whose divergence leads to the integrable functions required to obtain U. There exists no unique solution to this problem. Therefore, by means of the *Ostrogadksii formula*, one can transform Eqn. 4.1-4.3 into a set of $2D$ integral expressions. The Ostrogadksii formula is the expression of the divergence theorem of Gauss in rectangular form. Particularly, given a $3D$ volume U bounded by the surface S, an equivalent expression for the divergence theorem can be the following [156, 157]:

$$\begin{aligned} &\int\int\int_U \left(\frac{\partial Q}{\partial x} \;+\; \frac{\partial R}{\partial y} \;+\; \frac{\partial Z}{\partial z}\right) dxdydz \;= \\ &\int\int_S \left[Q\cos(\mathbf{n}, \mathbf{x}) \;+\; R\cos(\mathbf{n}, \mathbf{y}) \;+\; Z\cos(\mathbf{n}, \mathbf{z})\right] d\sigma, \end{aligned} \tag{4.5}$$

where $d\sigma$ is the element of the surface S; Q, R, Z are the components of the integrable function along the three axes (vector field); n is the normal of the surface; and x, y, z are the base vectors of the coordinate system. Q, R and Z can be expressed under Eqn. 4.4 definition,

$$Q = \frac{x_1}{2l},\ R = \frac{x_2}{2l},\ Z = \frac{x_3}{2l}. \tag{4.6}$$

When Eqn. 4.5 and Eqn. 4.6 are combined, Eqn. 4.1 - 4.3 are then expresesd like this,

$$U \ = \ \frac{G\rho}{2} \int\int_S \frac{1}{l} \left[x_1 \cos(\mathbf{N_p}, \mathbf{e_1}) \ + \ x_2 \cos(\mathbf{N_p}, \mathbf{e_2}) \ + \ x_3 \cos(\mathbf{N_p}, \mathbf{e_3}) \right] dS, \tag{4.7}$$

$$U_{x_i} \ = \ G\rho \int\int_S \frac{1}{l} \cos(\mathbf{N_p}, \mathbf{e_i}) dS, \ (i = 1, 2, 3), \tag{4.8}$$

$$U_{x_i x_j} \ = \ G\rho \int\int_S \frac{\partial}{\partial x_j} \left(\frac{1}{l} \right) \cos(\mathbf{N_p}, \mathbf{e_i}) dS, \ (i, j = 1, 2, 3). \tag{4.9}$$

As Gellert discussed, the previous expressions are algebraically related with the Hessian normal form of the equation of a plane [158]. The equation of a plane is $Ax + By + Cz + D = 0$, where the plane equation constants can adopt an infinite set of values. Moreover, as the numerical value are not relevant determining the geometry of the plane, the Hessian normal form is utilized. Normal vectors are required to use the Hessian normal form

$$n_1 = \frac{A}{\sqrt{A^2 + B^2 + C^2}},\ n_2 = \frac{B}{\sqrt{A^2 + B^2 + C^2}},\ n_3 = \frac{B}{\sqrt{A^2 + B^2 + C^2}}. \tag{4.10}$$

Each normal vector represents the direction cosines of the perpendicular that falls to the plane, from the coordinate system's origin. Furthermore, $p = \dfrac{D}{\sqrt{A^2 + B^2 + C^2}}$ provides the perpendicular's distance. Normally, a positive sign is assigned to p if it lies in the direction of the plane's unit normal vector, $\mathbf{n} = n_1\mathbf{e_1} + n_2\mathbf{e_2} + n_3\mathbf{e_3}$. If it lies in the other direction, then p will have a negative sign. For the model used in this study, outside-pointing unit normals are solely used. As a result, the Hessian normal form used will be

$$\cos(\mathbf{n}, \mathbf{e_1})x_1 \ + \ \cos(\mathbf{n}, \mathbf{e_2})x_2 \ + \ \cos(\mathbf{n}, \mathbf{e_3})x_3 \ \pm \ p \ = \ 0. \tag{4.11}$$

For nomenclature purposes, n is interchanged for N_P and p to h_p making reading easier. Their meanings have not changed,

$$\cos(\mathbf{N_p}, \mathbf{e_1})x_1 \ + \ \cos(\mathbf{N_p}, \mathbf{e_2})x_2 \ + \ \cos(\mathbf{N_p}, \mathbf{e_3})x_3 \ \pm \ h_p \ = \ 0. \tag{4.12}$$

As it can be noted, Eqn. 4.12 carries the same transcendental expressions than Eqn. 4.7 - 4.9. Therefore, the latter can be simplified

$$U \ = \ \frac{G\rho}{2} \sum_{p=1}^{n} \sigma_p h_p \int\int_S \frac{1}{l} dS, \tag{4.13}$$

$$U_{x_i} \ = \ \frac{G\rho}{2} \sum_{p=1}^{n} \mathbf{N_p}, \mathbf{e_i} \int\int_S \frac{1}{l} dS, \ (i = 1, 2, 3), \tag{4.14}$$

$$U_{x_i x_j} \ = \ G\rho \sum_{p=1}^{n} \cos(\mathbf{N_p}, \mathbf{e_i}) \int\int_S \frac{\partial}{\partial x_j} \left(\frac{1}{l} \right) dS, \ (i, j = 1, 2, 3). \tag{4.15}$$

being $\sigma_p = -1$ when N_p points to the half-space containing point P. What was initially troublesome, has now been solved with Eqn. 4.13 - 4.15. Ultimately, these expressions must be solved. To do that, the following tools are available: the divergence theorem is once again used. It produces n line integrals along each polygonal line of each face. Then, the analytical expression is studied, producing the final formulas, with relevant work provided by Tsoulis [67].

Ultimately, the closed formulas for the potential, the gravitation vector and the tensor of the second-order derivatives, are respectively as follows:

$$U \ = \ \frac{G\rho}{2} \sum_{p=1}^{n} \sigma_p h_p \left[\sum_{q=1}^{m} \sigma_{pq} h_{pq} LN_{pq} \ + \ h_p \ \sum_{q=1}^{m} \sigma_{pq} AN_{pq} \ + \ sing_{A_p} \right] \ , \tag{4.16}$$

$$
\begin{aligned}
U_{x_i} \;=\; & G\rho \sum_{p=1}^{n} \cos(\mathbf{N}_p, \mathbf{e}_i) \\
& \cdot \left[\sum_{q=1}^{m} \sigma_{pq} h_{pq} LN_{pq} \;+ h_p \; \sum_{q=1}^{m} \sigma_{pq} AN_{pq} \;+\; sing_{A_p} \right] \; (i = 1, 2, 3),
\end{aligned}
\tag{4.17}
$$

$$
\begin{aligned}
U_{x_i x_j} \;=\; & G\rho \sum_{p=1}^{n} \cos(\mathbf{N}_p, \mathbf{e}_i) \\
& \cdot \left[\sum_{q=1}^{m} \cos(\mathbf{n}_{pq}, \mathbf{e}_j) LN_{pq} \;+\; \sigma_p \cos(\mathbf{N}_p, \mathbf{e}_i) \; \sum_{q=1}^{m} \sigma_{pq} AN_{pq} \;+\; sing_{B_{pj}} \right], \\
& (i.j = 1, 2, 3).
\end{aligned}
\tag{4.18}
$$

Here, p refers to the plane defined by each polygonal surface S_p. Meanwhile, q stands for the polyhedral segments, and runs from 1 to m for each face p, where m denotes the variable number of maximum segments for every face. The parameter n_{pq} is the value of the normal vector of the segment q that lies on the plane of the polygon S_p. It points outside the closed polygonal surface S_p by definition. The position of the computation point P projected on the plane of each face with respect to S_p, $P^{'}$, is critical information for each face. If n_{pq} points to the half-plane that does not contain $P^{'}$, then $\sigma_{pq} \;=\; +1$. Else, $\sigma_{pq} \;=\; -1$. Furthermore, h_{pq} denotes the positive distance between $P^{'}$ and the line of each segment. Meanwhile, $\cos(\mathbf{n}_{pq}, \mathbf{e}_j)$ is the direction cosine between $\mathbf{n}_{pq}$ and the unit vector $\mathbf{e}_j$ of the unit vector triad situated at P. The values LN_{pq} and AN_{pq} are abbreviations of the following expressions:

$$
LN_{pq} \;=\; ln \frac{s_{2_{pq}} \;+\; l_{2_{pq}}}{s_{1_{pq}} \;+\; l_{1_{pq}}} \;, \tag{4.19}
$$

$$
AN_{pq} = \arctan \frac{h_p s_{2_{pq}}}{h_{pq} l_{2_{pq}}} \;-\; \arctan \frac{h_p s_{1_{pq}}}{h_{pq} l_{1_{pq}}} \tag{4.20}
$$

where $l_{1_{pq}}$ and $l_{2_{pq}}$ are the 3D distances between P and the end points of segment pq as it has been represented in Fig. 4.1, from Tsoulis' work [67]. With $P^{''}$ being the origin of a $1D$ local coordinate system defined on the line of segment pq, $s_{1_{pq}}$ and $s_{2_{pq}}$ are the $1D$ distances between $P^{''}$ and the two segment end points. In these definitions, subscript 1 always stands for the end, and subscript 2 is for the beginning of the corresponding segment vector [159]. Finally, the terms $sing_{A_p}$ and $sing_{B_{pj}}$ are the singularity terms that appear for specific locations of $P^{'}$ with

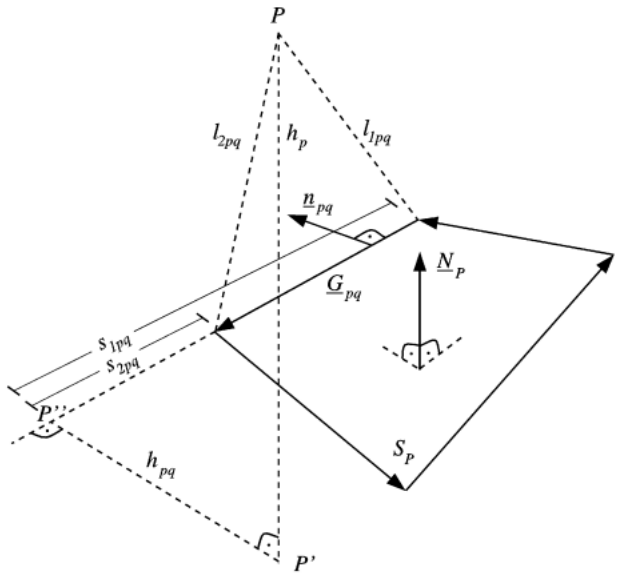

Figure 4.1: Geometrical defintions of an individual polyhedron face. [67]

respect to the polygonal line G_p when one attempts to apply the divergence theorem of Gauss for these cases. They express the analytical solutions of the corresponding limiting values of the line integrals that are obtained from the partial application of the divergence theorem for a small circle containing the singularity point when its radius tends towards zero. Tsoulis then showed the values of the three cases when (a) $P^{'}$ lies inside S_p, (b) $P^{'}$ is located on G_p, but not at any of its vertices and (c) $P^{'}$ is located at one of G_p's vertices [67]. When $P^{'}$ is located outside S_p, then $sing_{A_p} = sing_{B_{pj}} = 0$.

The developed final expressions are independent of the two coordinate transformations that took place for every face in the derivation process. They are given through two summations (one running over segments and the other over faces) of the same transcendental expressions that are directly linked to the end points of the individual segments (the polyhedral vertices). It is not necessary to deal explicitly with the intervening coordinate transformations because these are obsolete to the final expressions. The key for the success of programming these formulas is to secure the permanent knowledge of the relative position of points P, $P^{'}$, and $P^{''}$ with respect to every polygonal surface S_p of the closed polyhedral surface S. The implementation of this task can be performed in the program with the help of standard tools of vector calculus as shown in [160].

4.3 Algorithm Used

Tsoulis created a script to implement the algorithm developed, required to compute the gravitational potential, first-order derivatives, and the full gradiometric tensor at any given arbitrary point due to a constant density polyhedron [160]. FORTRAN was chosen as the programming language in which to present and develop the algorithm. To solve Eqn. 4.16 - 4.18 an ASCII file is required with the data of the geometric topology, described as $3-D$ coordinates (x, y, z). There must be n

records, meaning one per face, with all the polyhedral vertices and the connectivity of the vertices. Each record must numerate the vertices in the order in which the vertex coordinates are given. If the ASCII is to be constructed there are some useful tools available, such as *convhulln* in MATLAB, or more complex algorithms such as those referred to in [161].

4.3.1 243 Ida Data Collection

Thanks to all the historical SSSB observation missions accomplished, the shape of various asteroids and planetary moons has been constructed. The optical shape models have been derived through spacecraft imaging, distinct to those based on more inaccurate radar observations. The *EAR-A-5-DDR-RADARSHAPE-MODELS-V1.0* has been used to build the models [119]. The shape models use the cartographic coordinate system defined by the IAU's Working Group on Cartographic Coordinates [162]. Within the data set, asteroid 243 Ida's optical shape model data can be found too. However, it must be modified before it can be introduced into the code, as it is presented in Fig.4.2, for the moment incompatible with the FORTRAN program. The parameters f indicates the $3-D$ geometric position of the face, and v indicates the correspondent vertices used to create the faces.

```
v  2.660810e-01  1.160000e-04  3.619600e-02
v  2.703620e-01  2.061600e-02  2.005300e-02
v  2.528360e-01  4.380300e-02  4.348000e-02
v  2.238610e-01  3.499900e-02  7.403900e-02
v  2.282490e-01  7.574300e-02  3.457200e-02
v  2.217470e-01  8.976400e-02  1.835900e-02
v  1.963310e-01  1.037530e-01  3.861700e-02
v  1.719220e-01  1.276280e-01  1.760000e-04
v  1.308890e-01  1.388380e-01  2.981200e-02
v  1.052200e-01  1.459240e-01  1.090000e-04
```

(a)

```
v  2.216950e-01  7.174000e-03  8.262300e-02
v  2.161610e-01  1.114800e-02  8.510200e-02
v  2.321530e-01  1.009400e-02  7.564100e-02
v  2.299210e-01  1.812100e-02  7.573600e-02
v  2.260300e-01  2.525900e-02  7.634100e-02
f  1528  1527   260
f  1531   260  1527
f  1533  1532   263
f  1535   263  1532
f  1537  1536   266
```

(b)

```
f  2197   699  2195
f   699  2198  2195
f  2195  2198  2199
f  2198   698  2199
f    99  2202  2201
f  2201  2202  2200
f  2202   703  2200
f   703  2203  2200
f  2200  2203  2204
f  2203   702  2204
```

(c)

Figure 4.2: Example of original data of asteroid 243 Ida from EAR-A-5-DDR-RADARSHAPE-MODELS-V1.0 data set.

4.3.2 243 Ida Data Manipulation

Tsoulis named the program developed *polyhedron.f*. The program calculates all the terms from the expressions Eqn. 4.16 - 4.18.These quantities are computed automatically with the use of three files:

- File "xyzposnew" states the number of vertices and contains the coordinates of the i vertices, (x_i, y_i, z_i) of the polyhedron.
- File "topoaut" provides information on the number of vertices each face has.
- File "dataut" states the number faces and declares the number of edges used in each plane, in the same order as in "topoaut".

Fig. 4.3 is an example cube, showing how the files stated would look like.

Subsequently, asteroid 243 Ida's data obtained from [119], looks how it has been

```
file 'xyzposnew':

  10  10  20
  30  10  20
  30  20  20
  10  20  20
  10  10  10
  30  10  10
  30  20  10
  10  20  10

file 'topoaut':

  1 2 4
  2 3 4
  6 5 8 7
  8 5 1 4
  6 7 3 2
  5 6 2 1
  7 8 4 3

file 'dataut':

  3 3 4 4 4 4 4
```

Figure 4.3: Example cube used for the FORTRAN program, showing the format of the files required to run it.

presented in 4.3.1. Using simple tools from Excel, the data has been modified into three different files, as required. Finally, the program is run with the asteroid's data as input. Meanwhile, Fig. 4.4 shows the modified files containing asteroid 243 Ida's data points, compatible with the FORTRAN program, ready to be utilized.

```
1 2 3
1 3 4
1 4 5
1 5 6
1 6 7
1 7 8
1 8 9
1 9 10
1 10 11
1 11 12
1 12 13
1 13 14
1 14 15
1 15 16
1 16 17
1 17 18
1 18 19
```

(a) File ”xyzposnew”.

```
-8.595027 -2.142981 9.837974
-8.512944 -2.441047 9.835596
-8.396666 -2.728242 9.805350
-8.277033 -3.012594 9.782536
-8.139121 -3.288418 9.749317
-7.979787 -3.552830 9.701161
-7.803904 -3.806218 9.643047
-7.618460 -4.050807 9.582853
-7.427248 -4.288123 9.524887
-7.224893 -4.514614 9.461794
-7.013896 -4.730932 9.396100
-6.779718 -4.925753 9.307146
-6.538140 -5.108155 9.214773
-6.295759 -5.282769 9.127602
-6.053058 -5.450198 9.046153
-5.809632 -5.610297 8.969684
-5.568742 -5.766601 8.903247
-5.334279 -5.924317 8.853753
-5.102683 -6.081140 8.816447
-4.868560 -6.231473 8.782560
-4.632426 -6.375988 8.752908
-4.395486 -6.516576 8.729871
-4.160455 -6.658119 8.719541
-3.924518 -6.797464 8.717237
```

(b) File ”topoaut”.

```
3 3 3 3 3 3 3 3 3 3 3 3 3 3 3 3 3 3 3
3 3 3 3 3 3 3 3 3 3 3 3 3 3 3 3 3 3 3
3 3 3 3 3 3 3 3 3 3 3 3 3 3 3 3 3 3 3
3 3 3 3 3 3 3 3 3 3 3 3 3 3 3 3 3 3 3
3 3 3 3 3 3 3 3 3 3 3 3 3 3 3 3 3 3 3
3 3 3 3 3 3 3 3 3 3 3 3 3 3 3 3 3 3 3
3 3 3 3 3 3 3 3 3 3 3 3 3 3 3 3 3 3 3
3 3 3 3 3 3 3 3 3 3 3 3 3 3 3 3 3 3 3
3 3 3 3 3 3 3 3 3 3 3 3 3 3 3 3 3 3 3
3 3 3 3 3 3 3 3 3 3 3 3 3 3 3 3 3 3 3
3 3 3 3 3 3 3 3 3 3 3 3 3 3 3 3 3 3 3
3 3 3 3 3 3 3 3 3 3 3 3 3 3 3 3 3 3 3
3 3 3 3 3 3 3 3 3 3 3 3 3 3 3 3 3 3 3
3 3 3 3 3 3 3 3 3 3 3 3 3 3 3 3 3 3 3
3 3 3 3 3 3 3 3 3 3 3 3 3 3 3 3 3 3 3
3 3 3 3 3 3 3 3 3 3 3 3 3 3 3 3 3 3 3
3 3 3 3 3 3 3 3 3 3 3 3 3 3 3 3 3 3 3
3 3 3 3 3 3 3 3 3 3 3 3 3 3 3 3 3 3 3
```

(c) File ”dataut”.

Figure 4.4: Compatible data files of asteroid 243 ready to run in FORTRAN program.

A program in FORTRAN presented by Tsoulis computes the gravitational potential, its first-order derivatives and the full gradiometric tensor at arbitrary space points due to a general polyhedral source of constant density [159]. The program has been applied to asteroid 243 Ida. The results for the gravitational potential are presented in 4.4.

4.4 Results - Full Gravity Tensor of 243 Ida

Once run, the computed results from asteroid 243 Ida's data are obtained. The program computed the gravitational potential, the first-order derivatives and the full graviometric tensor at any arbitray point in space.

The graviometric tensor is as follows

$$\begin{pmatrix} V_{xx} & V_{xy} & V_{xz} \\ V_{xy} & V_{yy} & V_{yz} \\ V_{xz} & V_{yz} & V_{zz} \end{pmatrix} = \begin{pmatrix} +1.489721E-04 & +3.166483E-05 & -3.953275E-06 \\ +3.166483E-05 & -1.48972E-04 & +1.859060E-05 \\ -3.953275E-06 & +1.859060E-05 & -2.267133E-08 \end{pmatrix}, \tag{4.21}$$

where the values are expressed in J. The quantities will later be included in Chapter 5, where the orbital equations of motion and conserved quantities will be presented and discussed in further detail.

The results for the gravitational potential are demonstrated in Fig. 4.5 as contour maps of the gravitational force. The color code resembles the intensity of the gravitational potential, and its force in each of the three planes (xy, xz, yz). As can be seen from Fig. 4.5, the gravitational force follows the asteroid's shape accurately with its irregularities.

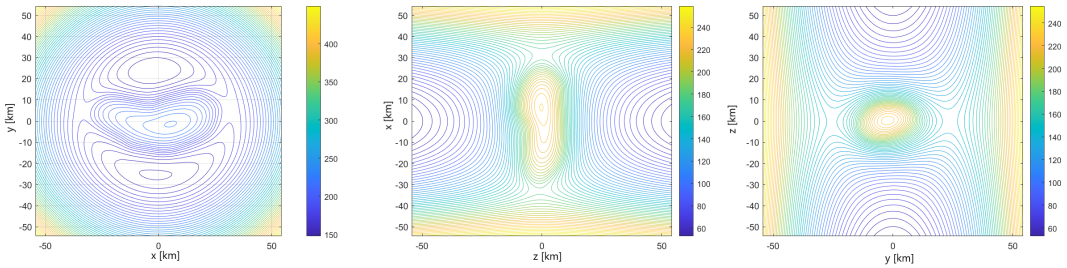

(a) (b) (c)

Figure 4.5: Contour plots of the gravitational potential of asteroid 243 Ida in $[m^2/s^2]$. Representations in (a) xy, (b) xz, (c) yz planes.

Chapter 5

Equations of Motion and Conserved Quantities

5.1 Equations of Motion

The motion equations of a mass point in the vicinity of a small celestial body (within radius R_3, explained in 3.1) are studied in this section. The irregular gravitational field calculated with the polyhedral model is considered. The frames employed are defined as follows:

1. Mass center body-fixed frame Oxyz: origin at mass center O, with axes x, y, z as the principal axes of minimum, medium and maximum inertia, respectively, forming a right-handed system.

2. Mass center inertia frame OXYZ: translational frame with origin at the center of mass of the small body O, with axis X pointing at J2000 mean equinox, XY plane parallel to Earth's orbital plane, and axes X, Y, Z forming a right-handed system.

Considering a massless point, the gravity from the mass point has no influence on the small celestial body. Therefore, the motion equation of the mass point is:

$$\frac{d^2}{dt^2}\mathbf{r} \;=\; -\nabla U, \tag{5.1}$$

which is the same as

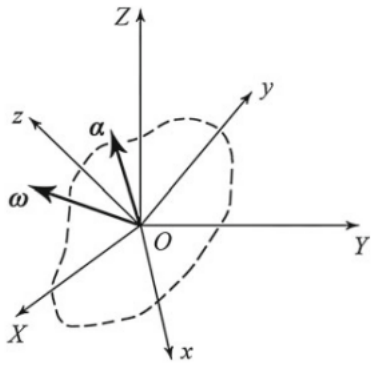

Figure 5.1: Frames and orbital characteristics of a SSSB.

$$\frac{d^2}{dt^2}\mathbf{r} \;+\; \frac{\partial U(\mathbf{r})}{\partial \mathbf{r}} \;=\; 0, \tag{5.2}$$

but is used to ease reading. If the left-hand side of the equation is expressed in relative derivatives, it provides:

$$\ddot{\mathbf{r}} \;+\; 2\omega \times \dot{\mathbf{r}} \;+\; \omega \times (\omega \times \mathbf{r}) \;+\; \alpha \times \mathbf{r} \;+\; \frac{\partial U(\mathbf{r})}{\partial \mathbf{r}} \;=\; 0, \tag{5.3}$$

Here, ω is the body's angular velocity (the asteroid's rotation rate), α is the body's angular acceleration, d/dt is the absolute derivative about time, " $\dot{}$ " is the relative derivative about time, and ∇U is the gravitational potential. Moreover, according to Pravec et al. most small bodies rotate around the principal axis and the variation of the angular velocity is as a result, slow [163]. Therefore, it is assumed for asteroid 243 Ida that the body's angular acceleration is equal to 0 ($\alpha = 0$), meaning that the asteroid will only revolve around its axis of maximum inertia, z ($\omega = (0, 0, \omega_z)$). This results into a simplification of the equation:

$$\ddot{\mathbf{r}} \;+\; 2\omega \times \dot{\mathbf{r}} \;+\; \omega \times (\omega \times \mathbf{r}) \;=\; -\frac{\partial U(\mathbf{r})}{\partial \mathbf{r}}. \tag{5.4}$$

The gravitational force acceleration is the gradient of *U(**r**)*, which is the gravitational potential of the asteroid. Where U($\mathbf{r}$) is calculated by the polyhedron model as

$$U(\mathbf{r}) \;=\; -\frac{1}{2}G\sigma \sum_{e \in edges} \mathbf{r}_e \cdot \mathbf{E}_e \cdot \mathbf{r}_e \cdot L_e \;+\; \frac{1}{2}G\sigma \sum_{f \in faces} \mathbf{r}_f \cdot \mathbf{E}_f \cdot \mathbf{r}_f \cdot L_f \cdot \omega_f. \tag{5.5}$$

So the gradient of the gravitational potential will be

$$\frac{\partial U(\mathbf{r})}{\partial \mathbf{r}} \;=\; \nabla U \;=\; G\sigma \sum_{e \in edges} \mathbf{r}_e \cdot \mathbf{E}_e \cdot L_e \;-\; G\sigma \sum_{f \in faces} \mathbf{F}_f \cdot \mathbf{r}_f \cdot \omega_f. \tag{5.6}$$

Finally, the motion equation can be fully extended as

$$\ddot{\mathbf{r}} \;+\; 2\omega \times \dot{\mathbf{r}} \;+\; \omega \times (\omega \times \mathbf{r}) \;=\; -G\sigma \sum_{e \in edges} \mathbf{r}_e \cdot \mathbf{E}_e \cdot L_e \;+\; G\sigma \sum_{f \in faces} \mathbf{F}_f \cdot \mathbf{r}_f \cdot \omega_f. \tag{5.7}$$

To simplify the previous equation, the effective potential of a rotating body is introduced. It is the sum of the centrifugal potential energy with the potential energy, U, of a dynamical system. It will allow the problem to be reduced to fewer dimensions hence, simplifying it. The formula for the effective potential is as follows

$$V \;=\; -\frac{1}{2}(\omega \times \mathbf{r}) \cdot (\omega \times \mathbf{r}) \;+\; U. \tag{5.8}$$

Taking into account that the rotational angular velocity vector only has a component in z for asteroid 243 Ida, $\omega = (0, 0, \omega_z)$, the effective potential can be rewritten as

$$V(x, y, z) \;=\; U(x, y, z) \;-\; \frac{1}{2}\omega^2(x^2 + y^2). \tag{5.9}$$

Therefore, the minor body's gradient of the effective potential at the relative position $\mathbf{r} = (x, y, z)^T$ can be expressed as:

$$\begin{aligned} \frac{\partial V(\mathbf{r})}{\partial x} &= \frac{\partial U(\mathbf{r})}{\partial x} \;-\; \omega^2 x, \\ \frac{\partial V(\mathbf{r})}{\partial y} &= \frac{\partial U(\mathbf{r})}{\partial y} \;-\; \omega^2 y, \\ \frac{\partial V(\mathbf{r})}{\partial z} &= \frac{\partial U(\mathbf{r})}{\partial z} \end{aligned} \tag{5.10}$$

This potential greatly simplifies the equation of motion:

$$\ddot{\mathbf{r}} \ + \ 2\omega \times \dot{\mathbf{r}} \ = \ -\nabla V. \tag{5.11}$$

When Eqn. 5.8 is derived, the potential of the efficient potential can be express as

$$\nabla V \ = \ \nabla U \ - \ \omega \times (\omega \times \mathbf{r}). \tag{5.12}$$

If the gradient of the efficient potential is expressed as a function of the gradient of the gravitational potential from Eqn. 5.6 and is combined with the definition of the efficient potential Eqn. 5.12

$$\nabla V \ = \ G\sigma \sum_{e \in edges} \mathbf{r}_e \cdot \mathbf{E}_e \cdot L_e \ - \ G\sigma \sum_{f \in faces} \mathbf{F}_f \cdot \mathbf{r}_f \cdot \omega_f - \ \omega \times (\omega \times \mathbf{r}). \tag{5.13}$$

The former expression will be used in the next section to iterate for the equilibrium point.

5.2 Equilibrium Points

5.2.1 Introduction

In physics, an equilibrium point is a point in space in a body-fixed frame *Oxyz* where the gravity from the body and the centrifugal force balance. For an SSSB, i.e. 243 Ida, which has an irregular appearance, the equilibrium points are usually of finite number and isolated. The equilibria may be key to understand the system dynamic behaviors, not only because of its simplicity, but also because it helps understanding global orbital behaviors. An equilibrium point will also be a critical point of the contour surfaces of the efficient potential V.

The asteroid 243 Ida is the specific example within this study. First, the equilibrium points of the asteroid using the polyhedral gravity model are found and the geometry of and topology of the contour surfaces of efficient potential V are presented. Then, using the linearized theory the stability and type of the equilibrium points are discussed.

5.2.2 Equilibrium Points of 243 Ida

To be able to solve the non-linear Eqn. 5.13, one must guess the initial values of the equilibrium points. To help assess the former, Fig. 4.5 is analyzed. A reasonable region for the initial guess is determined through the following analysis:

1. Equilibrium points are critical points of the efficient potential.

2. As asteroid 243 Ida is basically symmetric about the equatorial plane (xy), and the centrifugal force is always considered parallel to the equator, the z component of the resultant can only disappear when the point is close to the equatorial plane.

3. Centrifugal force is a radial force that acts in the direction of $\mathbf{r}$, while the asteroid's gravity that balances the centrifugal force must point in the opposite direction, towards the body center O. They must be around the x and $yaxis$.

Using the computed gravitational potential from Chapter 4, and supposing we are on the xy plane ($z = 0$), the following Fig. 5.2 is obtained.

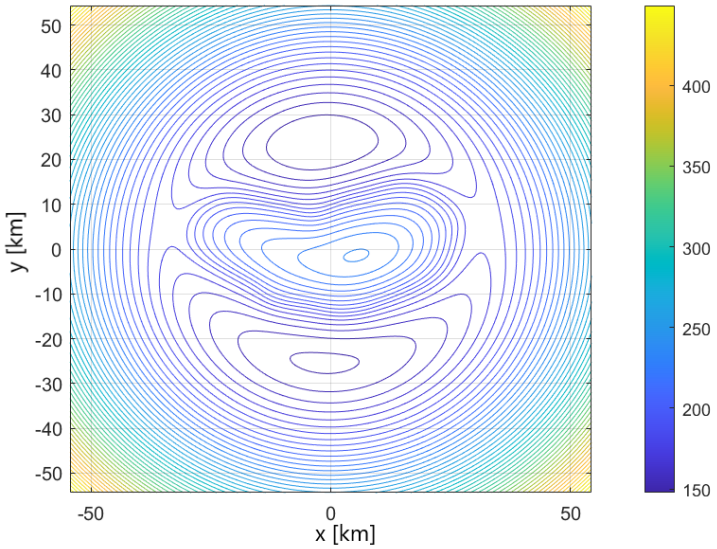

Figure 5.2: Contour plot of asteroid 243 Ida's efficient potential from polyhedron model in the xy plane. Axes units are $[km]$ and the efficient potential in $[m^2/s^2]$.

From Fig. 5.2 it can be appreciated that the equilibrium points will most likely be located near the lines of $x = 0$, $z = 0$, and the center of the asteroid as they present local minimums of the efficient potential in the contour plot. Thus, the initial guesses are plotted in Fig. 5.3

Once the initial guess is estimated, the following is remembered:

- The x, y, z axes correspond to the smallest, intermediate, and biggest moments of inertia respectively.

- It has been assumed that the asteroid has a uniform rotation around the z-axis.

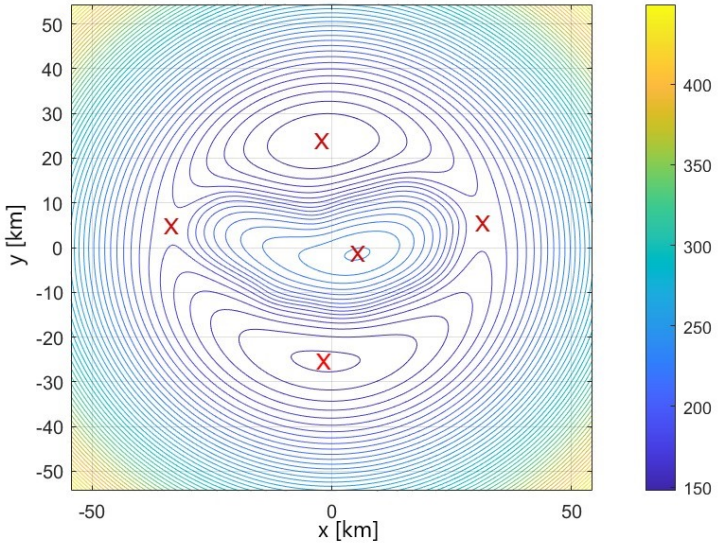

Figure 5.3: Estimation of the equilibrium points in the contour plot of asteroid 243 Ida's efficient potential from polyhedron model in the xy plane. Axes units are $[km]$ and the efficient potential in $[m^2/s^2]$.

Thus, $\omega = (0, 0, \omega)$, and $\dot{\omega} = 0$. To calculate the positions of the equilibrium points, it is assumed that the acceleration and velocity at those points will be 0. Therefore, $\ddot{\mathbf{r}} = \dot{\mathbf{r}} = 0$. As a consequence, the equilibrium points will satisfy the following equation:

$$\nabla V(x, y, z) \; = \; 0. \tag{5.14}$$

Therefore, Eqn. 5.13, 5.14 are combined to present the expression to be computed

$$G\sigma \sum_{e \in edges} \mathbf{r}_e \cdot \mathbf{E}_e \cdot L_e \; - \; G\sigma \sum_{f \in faces} \mathbf{F}_f \cdot \mathbf{r}_f \cdot \omega_f - \; \omega \times (\omega \times \mathbf{r}) \; = \; 0, \tag{5.15}$$

which can be further simplified to its final form

$$\sum_{e \in edges} \mathbf{r}_e \cdot \mathbf{E}_e \cdot L_e \; - \sum_{f \in faces} \mathbf{F}_f \cdot \mathbf{r}_f \cdot \omega_f - \; \frac{1}{G\sigma} \omega \times (\omega \times \mathbf{r}) \; = \; 0. \tag{5.16}$$

5.3 Stability of the Equilibrium Points

To be able to study the stability of each equilibrium point, motion has to be linearized into:

$$\ddot{\varepsilon} \; + \; A\dot{\varepsilon} \; + \; B\varepsilon \; = \; 0, \tag{5.17}$$

where $\varepsilon = [\xi, \eta, \zeta]^T$, and $\xi = x - x_E(t)$, $\eta = y - y_E(t)$, $\zeta = z - z_E(t)$. The location of the equilibrium point is defined as $[x_E, y_E, z_E]^T$. The linearized motion equations around the equilibrium points of the asteroid are

$$\begin{array}{rcl}
\ddot{\xi} \; + \; 2\omega_y\dot{\zeta} \; - \; 2\omega_z\dot{\eta} \; + \; V_{xx}\xi \; + \; V_{xy}\eta \; + \; V_{xz}\zeta \; = \; 0 \\
\ddot{\eta} \; + \; 2\omega_z\dot{\xi} \; - \; 2\omega_x\dot{\zeta} \; + \; V_{xy}\xi \; + \; V_{yy}\eta \; + \; V_{yz}\zeta \; = \; 0 \\
\ddot{\zeta} \; + \; 2\omega_x\dot{\eta} \; - \; 2\omega_y\dot{\xi} \; + \; V_{xz}\xi \; + \; V_{yz}\eta \; + \; V_{zz}\zeta \; = \; 0
\end{array} \tag{5.18}$$

Following the assumptions detailed in the prior sections, the motion equations can be simplified into

$$\begin{array}{rcl}
\ddot{\xi} \; - \; 2\omega\dot{\eta} \; + \; V_{xx}\xi \; + \; V_{xy}\eta \; + \; V_{xz}\zeta \; = \; 0 \\
\ddot{\eta} \; + \; 2\omega\dot{\xi} \; + \; V_{xy}\xi \; + \; V_{yy}\eta \; + \; V_{yz}\zeta \; = \; 0 \\
\ddot{\zeta} \; + \; V_{xz}\xi \; + \; V_{yz}\eta \; + \; V_{zz}\zeta \; = \; 0.
\end{array} \tag{5.19}$$

Thus, the linearized equations of motion relative to the equilibrium points of the asteroid can be expressed as the potential as

$$\frac{d^2}{d^2t}\begin{bmatrix} \xi \\ \eta \\ \zeta \end{bmatrix} \; + \; \begin{pmatrix} 0 & -2\omega & 0 \\ 2\omega & 0 & 0 \\ 0 & 0 & 0 \end{pmatrix} \cdot \frac{d}{dt}\begin{bmatrix} \xi \\ \eta \\ \zeta \end{bmatrix} \; + \; \begin{pmatrix} V_{xx} & V_{xy} & V_{xz} \\ V_{xy} & V_{yy} & V_{yz} \\ V_{xz} & V_{yz} & V_{zz} \end{pmatrix} \cdot \begin{bmatrix} \xi \\ \eta \\ \zeta \end{bmatrix} \; = \; 0, \tag{5.20}$$

where the matrix A and B are expressed as

$$A \; = \begin{pmatrix} 0 & -2\omega & 0 \\ -2\omega & 0 & 0 \\ 0 & 0 & 0 \end{pmatrix}, \quad B \; = \begin{pmatrix} V_{xx} & V_{xy} & V_{xz} \\ V_{xy} & V_{yy} & V_{yz} \\ V_{xz} & V_{yz} & V_{yz} \end{pmatrix}. \tag{5.21}$$

Referring back to Eqn. 5.17, the motion equation near the equilibrium point can be rewritten as

$$\begin{aligned} \dot{\varepsilon} &= \dot{\varepsilon} \\ \ddot{\varepsilon} &= -B\varepsilon - A\dot{\varepsilon} \end{aligned} \tag{5.22}$$

Remembering that the efficient potential can be expressed as noted in 5.12, matrix B can also be represented as

$$V_{\mathbf{rr}} \triangleq \begin{pmatrix} V_{xx} & V_{xy} & V_{xz} \\ V_{xy} & V_{yy} & V_{yz} \\ V_{xz} & V_{yz} & V_{zz} \end{pmatrix} = \nabla\nabla U - \Omega\Omega, \tag{5.23}$$

where Ω is

$$\Omega = \begin{pmatrix} 0 & -\omega_z & \omega_y \\ \omega_z & 0 & -\omega_x \\ -\omega_y & \omega_x & 0 \end{pmatrix}, \tag{5.24}$$

and $\Omega\Omega$ is

$$\Omega\Omega = \begin{pmatrix} 0 & -\omega_z & \omega_y \\ \omega_z & 0 & -\omega_x \\ -\omega_y & \omega_x & 0 \end{pmatrix} \begin{pmatrix} 0 & -\omega_z & \omega_y \\ \omega_z & 0 & -\omega_x \\ -\omega_y & \omega_x & 0 \end{pmatrix} = \begin{pmatrix} -\omega_y^2 - \omega_z^2 & \omega_x^2 & \omega_x\omega_z \\ \omega_x\omega_y & -\omega_x^2 - \omega_z^2 & \omega_y\omega_z \\ \omega_x\omega_z & \omega_y\omega_z & -\omega_x^2 - \omega_y^2 \end{pmatrix}. \tag{5.25}$$

Remembering that for asteroid 243 Ida it has been assumed that it only has rotational velocity in its principle axis of inertia (z), so $\omega_z = \omega$. Therefore, $\Omega\Omega$ can be rewritten as

$$\Omega\Omega = \begin{pmatrix} -\omega^2 & 0 & 0 \\ 0 & -\omega^2 & 0 \\ 0 & 0 & 0 \end{pmatrix}. \tag{5.26}$$

Going back to Eqn. 5.22, it can therefore be expressed as

$$\begin{aligned} \dot{\varepsilon} &= \dot{\varepsilon} \\ \ddot{\varepsilon} &= (-\nabla\nabla U + \Omega\Omega)\varepsilon - 2\Omega\dot{\varepsilon}\ , \end{aligned} \tag{5.27}$$

meaning that the coefficient matrix C can be expressed as

$$\mathbf{C} \;=\; \begin{pmatrix} \mathbf{0} & \mathbf{I} \\ -\nabla\nabla U + \Omega\Omega & -2\Omega \end{pmatrix}. \tag{5.28}$$

Being $\mathbf{0}$ a zero matrix and $\mathbf{I}$ an identity matrix, both of size 3. From the above Eqn. 5.28 one can see that the coefficient matrix $\mathbf{C}$ is of size 6. Therefore, solving the matrix will result in 6 eigenvalues. Thus, Eqn. 5.29 must be solved to find the eigenvalues $\lambda_i,\ (i = 1, ..., 6)$, such that

$$det(\mathbf{C} - \lambda\mathbf{I}) \;=\; \prod_{i=1}^{6}(\lambda - \lambda_i). \tag{5.29}$$

Substituting Eqn. 5.28 into Eqn. 5.29 yields the even polynomial provided in Eqn. 5.30

$$\lambda^6 \;+\; b_4\lambda^4 \;+\; b_2\lambda^2 + b_0 \;=\; 0, \tag{5.30}$$

where b_0, b_2, b_4 are real coefficients. As it is an even polynomial, the solution will satisfy the following:

- Two opposite real numbers.
- Two opposite imaginary numbers.
- Four opposite conjugate complex numbers.

It is necessary to remember that Eqn. 5.17 and 5.29 are both for uniformly rotating minor bodies. If there is a variation of the parameters, this will imply a change in the position, stability, and topological classification of the equilibrium points. Some of the parameters that can be altered are the rotational velocity, the density and the shape. Further work may look upon supposing a variation of the parameters, to identify how the equilibrium points differ with each parameter. It is out of the spectrum to analyze such cases in this study.

With Eqn. 5.29 and the full graviometric tensor obtained in Chapter 4, the equilibrium points are easily computed.

Equilibrium Points	x (km)	y (km)	z (km)
E1	31.3969	5.96274	0.0340299
E2	-2.16095	23.5734	0.0975084
E3	-33.3563	4.85067	-1.08844
E4	-1.41502	-25.4128	-0.378481
E5	5.43176	-1.41369	-0.144237

Table 5.1: Equilibrium points around asteroid 243 Ida in the body-fixed frame.

Where the eigenvalues of the equilibrium points around asteroid 243 Ida are expressed in the following Table 5.2

Equilibrium Points	λ_1	λ_2	λ_3	λ_4	λ_5	λ_6
E1	$0.51138i$	$-0.51138i$	$0.48606i$	$-0.48606i$	0.46213	-0.46213
E2	$0.38816i$	$-0.38816i$	$0.23774+0.35113i$	$0.23774-0.35113i$	$-0.23774+0.35113i$	$-0.23774-0.35113i$
E3	$0.59220i$	$-0.59220i$	$0.53867i$	$-0.53867i$	0.59723	-0.59723
E4	$0.39597i$	$-0.39597i$	$0.17581+0.30617i$	$0.17581-0.30617i$	$-0.17581+0.30617i$	$-0.17581-0.30617i$
E5	$1.1467i$	$-1.1467i$	$1.0377i$	$-1.0377i$	$0.27396i$	$-0.27396i$

Table 5.2: Eigenvalues computed corresponding to each equilibrium point around asteroid 243 Ida.

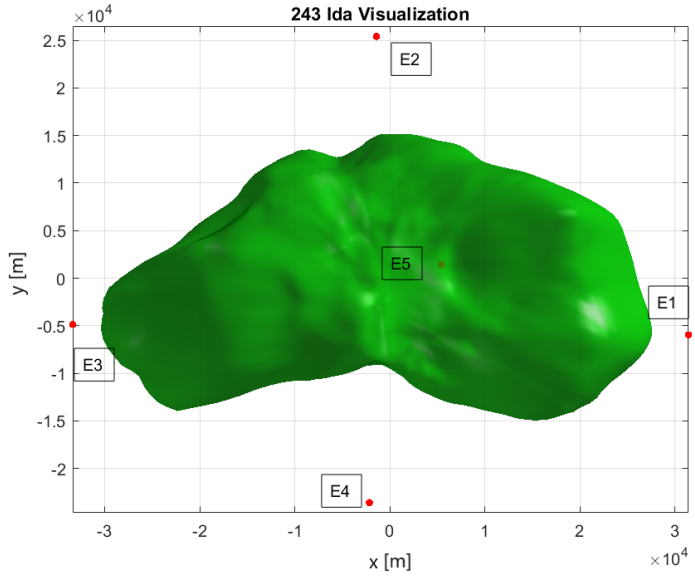

Figure 5.4: Equilibrium points of asteroid 243 Ida.

Once obtained the equilibrium points around 243 Ida, the stability of each can be determined. For an equilibrium point to be stable, the Hessian matrix of the effective potential, $\nabla^2 V$ must be positive definite. That is, the expression from Eqn. 5.23 must be positive definite.

5.3.1 Linear classification

To propose a linear classification of the equilibrium points, the matrix's rank must be introduced. The rank of a given matrix is the dimension of the vector space generated by its columns. This corresponds to the maximal number of linearly independent columns of the matrix. The Hessian matrix, $\nabla^2 V$ has full rank if and only if $det(\nabla^2 V) \neq 0$. Expressed simply, if and only if it has non-zero eigenvalues. Therefore, it is identical to the dimension of the vector space spanned by its rows. In this case, the Hessian matrix from 5.23 will be full rank if its rank is equal to three. On one hand, if it is full rank it will mean that the equilibrium point is non-degenerate. A non-degenerate equilibrium point means that the Hessian matrix has non-zero eigenvalues, whereas a degenerate will have zero eigenvalues. On the other hand, if the rank is less than three, the equilibrium point is degenerate, which corresponds to the case in which $det(\nabla^2 V) = 0$. The equilibrium points in the potential field of a rotating asteroid can be classified as non-degenerate linear or also known as degenerate linear.

5.3.2 Rank classification

Knowing the rank of the Hessian matrix is three, the equilibrium points can ve classified into $n = 3$ classes, being n the number of columns of the Hessian matrix. The rank of the matrix can be any of $n = 1, 2, 3$, and each value of the rank defines a class of the equilibrium points. Thus, an equilibrium point in the potential field of a rotating irregular minor celestial body has three rank classes. Each classification will be linked to different laws of motion when considering the dynamical evolution of a massless particle in the neighborhood of the equilibrium points. Jiang et al. theorized eight cases of equilibrium points in the potential field of a rotating asteroid that led to the topological manifold classification of the equilibrium points [164].

5.3.3 Topological manifold classification

Furthermore, equilibrium points can be classified into resonant and non-resonant points. The resonant equilibrium point is a Hopf bifurcation point when a parameter varies. The Hopf bifurcation can transfer into chaos, which leads to the chaotic motion near the resonant equilibrium point. As a result, periodic-orbit families appear and disappear around near resonant equilibrium points with parametric variation [165].

To simplify the work carried out, only non-degenerate and non-resonant equilibrium points are considered. Under these conditions, the topological manifold classification will result in the following table:

Where:

- C1: Case

C1	C2	C3	C4
Case 1	$\pm i\beta_j(\beta_j \in \mathbf{R}^+; j = 1, 2, 3)$	LS	3
Case 2	$\pm\alpha_j(\alpha_j \in \mathbf{R}^+; j = 1)$, $\pm i\beta_j(\beta_j \in \mathbf{R}^+; j = 1, 2)$	U	2
Case 3	$\pm\alpha_j(\alpha_j \in \mathbf{R}^+; j = 1, 2)$, $\pm i\beta_j(\beta_j \in \mathbf{R}^+; j = 1)$	U	1
Case 4a	$\pm\alpha_j(\alpha_j \in \mathbf{R}^+; j = 1)$, $\pm\sigma \pm i\tau(\sigma, \tau \in \mathbf{R}^+)$	U	0
Case 4b	$\pm\alpha_j(\alpha_j \in \mathbf{R}^+; j = 1, 2, 3)$	U	0
Case 5	$\pm\sigma \pm i\tau(\sigma, \tau \in \mathbf{R}^+)$, $\pm i\beta_j(\beta_j \in \mathbf{R}^+; j = 1)$	U	1

Table 5.3: The topological manifold classification of non-degenerate and non-resonant equilibrium points.

- C2: Eigenvalues (imaginary eigenvalues are different)
- C3: Stability of the equilibrium points

  U: Unstable

  LS: Linearly stable
- C4: Number of periodic orbit families around equilibrium points

Now that the topological manifold classification of equilibrium points has been presented, it can be applied to the equilibrium points around asteroid 243 Ida obtained previously to analyze their stability. The results are presented in the following table:

Equilibrium Points	Case	Stability	$\nabla^2 V$
E1	2	U	N
E2	5	U	P
E3	2	U	N
E4	5	U	P
E5	1	LS	P

Table 5.4: Topological manifold classification of the equilibrium points around asteroid 243 Ida.

Where $\nabla^2 V$ can be classified as:

- N: Non-positive definite
- P: Positive definite

From Table 5.4 can be seen that all equilibrium points except for E5 are unstable. In other words, every equilibrium point around asteroid 243 Ida exterior to the body is unstable. The instability of the equilibrium points must be taken into account in future research, when orbits around the equilibrium points are found, as it will likely generate different orbital families due to a different orbital dynamic characteristics.

Chapter 6

Additional Considerations and Future Directions

6.1 Limitations and Additional Considerations

Moreover, some limiting hypothesis of the polyhedron method utilized is assuming a constant density through the asteroid and a constant rotational velocity around its principal axis of inertia. To solve the constant density problem, a more complex model can be developed, were the dynamical factor is introduced.

As Pravec et al. analyzed, most celestial small bodies rotate around the principal axis, meaning that the variation of the angular velocity is slow [163]. Therefore, it has been assumed that the body's angular acceleration is equal to 0 ($\alpha = 0$). If this assumption was not to be made, it would not be possible to provide analytical equations allowing to solve the orbital motion equations of a massless point around a small body. However, Yu demonstrated and classified the vanishing of equilibrium points of asteroid 243 Ida with each other as the rotational velocity varies [166].

Furthermore, asteroid 243 Ida is part of a binary system. A simplifying hypothesis has overlooked the gravitational effect of Ida's moon, Dactyl. However magnitudes smaller the moon is to the main asteroid, it cannot be neglected when pretending to provide a precise calculation of equilibrium points and later on, orbital families around them.

6.1.1 Dynamical Factor κ

It is known that asteroids do not have a constant uniform density throughout its whole body. That is why assuming that they have a constant density is an over-simplification applied for the case studied. Therefore, the results obtained cannot be assumed to be exact. To analyze different bulk densities, Yu et al. developed

a dimensionless parameter named κ [110]. This parameter becomes an important indicator for the orbital behavior around the small body. Before an expression of the parameter is introduced, we must refer back to Eq. 5.3.

A dimensionless form of Eq. 5.3 is presented, taking the rotation period (T_A as the time scaler, and the equivalent radius as the length scaler:

$$[T] = T_A, [L] = \sqrt[3]{\frac{3V_A}{4\pi}}. \tag{6.1}$$

If the time is scaled, $\tau = t/[T]$, combined with Eqs. 5.3 and 5.6, the following expression results

$$\tilde{\mathbf{r}}'' + 4\pi\hat{\omega}\times\tilde{\mathbf{r}} + 4\pi^2\hat{\omega}\times(\hat{\omega}\times\tilde{\mathbf{r}}) = \kappa\left(\sum_{e\in ES}\tilde{\mathbf{r}}_e\cdot\mathbf{E}_e\cdot L_e - \sum_{f\in FS}\mathbf{F}_f\cdot\tilde{\mathbf{r}}_f\cdot\theta_f\right). \tag{6.2}$$

where $\ll\tilde{}\gg$ indicates the scaled length vector and $\ll'\gg$ indicates the relative derivative about the scaled time. Therefore, κ is defined as

$$\kappa = GT_A^2\sigma. \tag{6.3}$$

The bracketed right side of Eq. 6.2 corresponds to the polyhedral shape of the asteroid. Whereas, κ is a reflection of the influence of an SSSB's bulk density and rotational period. It describes the combined effect of the asteroidal gravity and the centrifugal force due to the asteroid's rotation. If κ has a large value, it corresponds to a large bulk density, or a slow rotational velocity. If κ has a small value, it signifies a small bulk density, or a fast rotational velocity.

Yu et al. checks the system dynamic's dependence on κ using asteroid 433 Eros as an example. Just like the study presented, the polyhedral shape model of Eros is utilized. In this case, the model contains 856 vertices and 1708 triangular faces. A common feature asteroid 433 Eros has with 243 Ida is its elongated shape. Having a narrow neck in the middle (said to be formed by a meteorite impact), and a box size of $11.87\times14.44\times32.74km$, proving to be a massive asteroid. According to mission NEAR Shoemaker, the data on the asteroid returned a bulk density of 2.67 g/cc, while it is rotating uniformly around the principal axes of maximum inertia, with period 5.27h.

Using different values of κ, it was studied its effect on the efficient potential, V. Contour lines of V are shown for various values of κ.

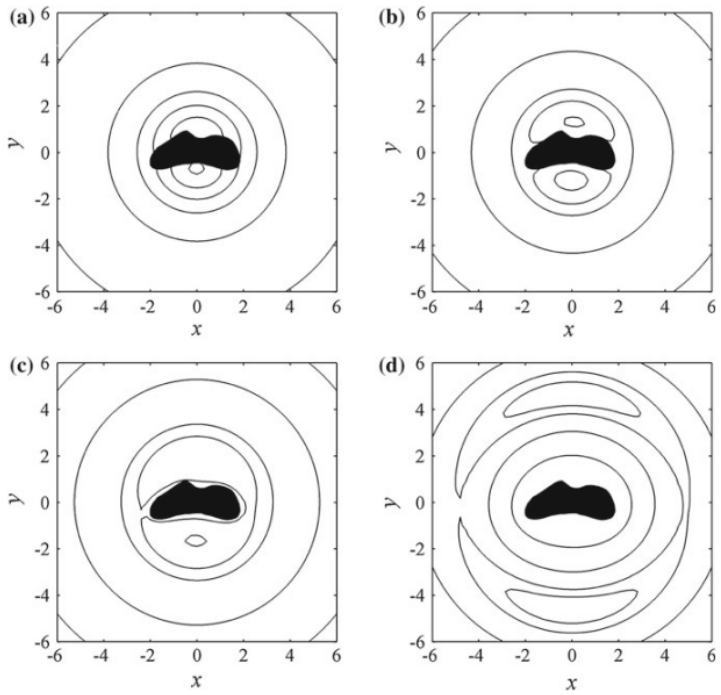

Figure 6.1: Variation of efficient potential with the dynamical factor κ for example asteroid 433 Eros. [110]

where (a)$\kappa = 10$, (b) $\kappa = 30$, (c) $\kappa = 64$, (d) $\kappa = 990$. The contour lines show singular points that indicate the stationary values of the function $V(x, y)$, also referred to as the equilibrium points throughout the thesis. As it can be shown in Fig. 6.1, when κ has the lowest value, case (a), there is only one equilibrium point in the exterior of the asteroid. When the value of κ is increased, case (b), the gravitational effect of the asteroid has become stronger, so two equilibrium points appear. When the value of κ is increased further, case (c) (close to its actual value, $\kappa = 64.10$), there exists 4 equilibrium points. Those close to the long axis are close to the surface. Therefore, the regolith material from the surface of the asteroid can stay on the surface due to its gravity. However, when κ is increased further to case (d) these equilibrium points are distanced from the surface, being far away from the asteroid.

This discussion leads to the study of the importance of the altitude of a stationary orbit. The altitude is the distance from the equilibrium to the surface of the small body. To some extent, it dictates the dynamics of the system. For an approximate analysis, if the asteroid is assumed to be a solid sphere of radius $[L]$, the altitude of the stationary orbit h satisfies

$$h = \left(\sqrt[3]{\frac{\kappa}{3\pi}} - 1 \right) [L]. \tag{6.4}$$

The altitude of the stationary orbit and κ show a correlation: if $\kappa \geq 3\pi$, then $h \geq 0$. In that case, the equilibrium points are located outside the target body, dividing regions dominated by the centrifugal force and the gravity. Most of the SSSBs are composed of rubble pile interiors. Therefore, bodies of $\kappa < 3\pi$ are rare in reality.

Ref. [110] lists in a table the values of κ of various asteroids, with their corresponding known bulk densities and rotational velocities. κ ranges from $15.79 - 1820.46$, with the majority being concentrated between $20 - 200$. The results confirm the rubble pile structure theory, when $\kappa \geq 3\pi$.

It can be concluded that the dynamical factor κ provides the following points:

- The value of κ determines the geometric properties of the efficient potential, and changes with κ.
- The value of κ determines the number and positions of the equilibrium points.
- A change in the bulk density can be vital to understand h and the equilibrium points. Therefore, proving the importance of an exact estimation of the density.

6.2 Future Directions

A possible future direction could be studying the large-scale periodic motion around the asteroid 243 Ida. It has already been done for other asteroids like 433 Eros [110]. It can be developed through different methods such as the Hierarchical Grid Search Method [167]. This method searches for periodic orbits around an irregular massive body. The stability of the orbits can also be calculated through the Poincare mapping, creating a discrete system. and the topological evolution of the orbital families can be studied.

If Dactyl's gravitational effect is taken into account, it would result in a new perturbation to be taken into account in the orbital dynamics experienced by a spacecraft around asteroid 243 Ida. A precise tracking (or imaging) system is required for orbital tracking, autonomous navigation and control of the spacecraft, and global trajectory optimization. Also, a new model must be built upon the addition of Dactyl's gravitational effect.

Furthermore, research could focus on finding about the existence of periodic orbits around the unstable equilibrium points found around asteroid 243 Ida. This could result in a better understanding of small celestial bodies as it is likely that most asteroids contain more than one unstable equilibrium point. This study could resemble research completed for the Lagrange points.

Finally, the effects of those forces not taken into account for this study, such as the variation in angular velocity, could be quantified. As an example, they could be computed with a numerical simulation that would identify the perturbed trajectory around an equilibrium point.

Chapter 7

Conclusion

The thesis has provided a deep understanding of the research status of orbital dynamics around a Solar System small body. Different missions have been compiled, selecting asteroid 243 Ida due to its academic interest and wide data available due to its extensive research. The asteroid's properties have been either compiled or computed. Then, detail on how to map the target SSSB's surface is presented, proving Galileo's importance. The data set utilized is presented as the most accurate up to date, containing 16022 vertices and 32040 faces. A general introduction to orbital dynamics is discussed, surveying the available methods to calculate the gravity of an irregular, demonstrating the advantages and drawbacks of each. The polyhedron method is chosen over harmonics, due to a more precise approach approximating the gravity of asteroid 243 Ida. The efficient potential is derived and contour plots are drawn, showing how the potential follows the irregular shape of the asteroid. The equilibrium points are computed, and their stability is analyzed. All exterior points are found to be unstable. Other orbital motions - such as periodic orbits or motion near the surface - should be considered. As for the polyhedral model, it is based on the assumption of working with a homogeneous polyhedron. Asteroids probably have non-uniform interior structure densities. A non-homogeneous polyhedral method should be developed to provide better approximations of the gravitation field. Finally, the rotational velocity and bulk density assumed may greatly affect the number, position and stability of equilibrium points around an irregular body through the dynamical factor κ.

Bibliography

[1] Nick Scoville et al. "COSMOS: Hubble space telescope observations". In: *The Astrophysical Journal Supplement Series* 172.1 (2007), p. 38.

[2] Dennis L Matson, Linda J Spilker, and Jean-Pierre Lebreton. "The Cassini/Huygens mission to the Saturnian system". In: *The Cassini-Huygens Mission* (2003), pp. 1–58.

[3] Michael JS Belton et al. "The discovery and orbit of 1993 (243) 1 Dactyl". In: *Icarus* 120.1 (1996), pp. 185–199.

[4] Clifford J Cunningham. "Introduction to asteroids: the next frontier". In: *Richmond* (1988).

[5] John Dankanich et al. "Main belt asteroid sample return mission design". In: *46th AIAA/ASME/SAE/ASEE Joint Propulsion Conference & Exhibit*. 2010, p. 7015.

[6] VS SAFRONOV. "Evolution of Protoplanetary Cloud and Formation of the Earth and Planets, Nauka, Moscow". In: *NASA Tech. Trans.* (1969), F–677.

[7] Stuart J Weidenschilling. "Formation of planetesimals and accretion of the terrestrial planets". In: *Space Science Reviews* 92.1 (2000), pp. 295–310.

[8] IAU (The International Astronomical Union) Minor Planet Center. `http://www.minorplanetcenter.net/mpc/summary`. 2013.

[9] NASA Space Science Data Coordinated Archive. *Phobos 2 Orbiter and Lander*. 1988. URL: `https://nssdc.gsfc.nasa.gov/nmc/spacecraft/display.action?id=1988-059A`.

[10] NASA Space Science Data Coordinated Archive. *Phobos 2*. 1988. URL: `https://en.wikipedia.org/wiki/Phobos_2`.

[11] NASA Space Science Data Coordinated Archive. *Galileo Mission*. 1993. URL: `https://nssdc.gsfc.nasa.gov/planetary/galileo.html`.

[12] NASA Space Science Data Coordinated Archive. *Asteroid 243 Ida raw image*. 1993. URL: `https://nssdc.gsfc.nasa.gov/imgcat/html/object_page/gal_0202561352.html`.

[13] NASA Space Science Data Coordinated Archive. *Asteroid Dactyl, 243 Ida moon*. 1993. URL: `https://nssdc.gsfc.nasa.gov/imgcat/html/object_page/gal_0202562278.html`.

[14] NASA Space Science Data Coordinated Archive. *Near Earth Asteroid Rendezvous (NEAR)*. 1996. URL: https://nssdc.gsfc.nasa.gov/nmc/spacecraft/display.action?id=1996-008A.

[15] NASA Space Science Data Coordinated Archive. *NEAR Shoemaker Spacecraft*. 1996. URL: https://en.wikipedia.org/wiki/NEAR_Shoemaker.

[16] NASA Space Science Data Coordinated Archive. *Asteroid 433 Eros*. 1996. URL: https://en.wikipedia.org/wiki/433_Eros.

[17] NASA Space Science Data Coordinated Archive. *Cassini orbiter and Hyugens Titan lander*. 1997. URL: https://nssdc.gsfc.nasa.gov/nmc/spacecraft/display.action?id=1997-061A.

[18] NASA Space Science Data Coordinated Archive. *Cassini Mission*. 1997. URL: https://en.wikipedia.org/wiki/Cassini%E2%80%93Huygens.

[19] NASA Space Science Data Coordinated Archive. *Huygens probe*. 1997. URL: https://nssdc.gsfc.nasa.gov/nmc/spacecraft/display.action?id=1997-061C.

[20] NASA Space Science Data Coordinated Archive. *Deep Space 1 mission*. 1998. URL: http://www.astronautix.com/d/deepspace1.html.

[21] NASA Space Science Data Coordinated Archive. *Hayabusa and Minerva mission*. 2003. URL: https://nssdc.gsfc.nasa.gov/nmc/spacecraft/display.action?id=2003-019A.

[22] NASA Space Science Data Coordinated Archive. *Hayabusa mission*. 2003. URL: https://en.wikipedia.org/wiki/Hayabusa.

[23] NASA Space Science Data Coordinated Archive. *MINERVA probe*. 2003. URL: https://en.wikipedia.org/wiki/MINERVA_(spacecraft).

[24] NASA Space Science Data Coordinated Archive. *Asteroid 25143 Itokawa*. 2003. URL: https://en.wikipedia.org/wiki/25143_Itokawa.

[25] NASA Space Science Data Coordinated Archive. *Rosetta orbiter and Philae lander*. 2004. URL: https://nssdc.gsfc.nasa.gov/nmc/spacecraft/display.action?id=2004-006A.

[26] NASA Space Science Data Coordinated Archive. *Rosetta orbiter*. 2004. URL: https://en.wikipedia.org/wiki/Rosetta_(spacecraft).

[27] NASA Space Science Data Coordinated Archive. *Philae lander*. 2004. URL: https://web.archive.org/web/20080920115856/http:/nssdc.gsfc.nasa.gov/nmc/spacecraftDisplay.do?id=PHILAE.

[28] NASA Space Science Data Coordinated Archive. *Comet 67P*. 2004. URL: https://en.wikipedia.org/wiki/67P/Churyumov-Gerasimenko.

[29] NASA Space Science Data Coordinated Archive. *Deep Impact impactor mission*. 2005. URL: https://nssdc.gsfc.nasa.gov/nmc/spacecraft/display.action?id=2005-001A.

[30] NASA Space Science Data Coordinated Archive. *Deep Impact spacecraft*. 2005. URL: https://en.wikipedia.org/wiki/Deep_Impact_(spacecraft).

[31] NASA Space Science Data Coordinated Archive. *Comet 9P*. 2005. URL: https://en.wikipedia.org/wiki/9P/Tempel.

[32] NASA Space Science Data Coordinated Archive. *Dawn mission*. 2007. URL: https://nssdc.gsfc.nasa.gov/nmc/spacecraft/display.action?id=DAWN.

[33] NASA Space Science Data Coordinated Archive. *Dawn mission, approach to 4 Vesta*. 2007. URL: https://en.wikipedia.org/wiki/Dawn_Mission.

[34] NASA Space Science Data Coordinated Archive. *Asteroid 4 Vesta*. 2007. URL: https://en.wikipedia.org/wiki/4_Vesta.

[35] NASA Space Science Data Coordinated Archive. *Dawn mission, approach to 1 Ceres*. 2007. URL: https://www.space.com/28754-nasa-dawn-ceres-dwarf-planet-arrival.html.

[36] NASA Space Science Data Coordinated Archive. *Asteroid 1 Ceres*. 2007. URL: https://en.wikipedia.org/wiki/Ceres_(dwarf_planet).

[37] NASA Space Science Data Coordinated Archive. *Hayabusa 2 mission*. 2014. URL: https://en.wikipedia.org/wiki/Hayabusa2.

[38] NASA Space Science Data Coordinated Archive. *MINERVA-II spacecraft*. 2014. URL: https://en.wikipedia.org/wiki/MINERVA-II.

[39] NASA Space Science Data Coordinated Archive. *MASCOT lander*. 2014. URL: https://en.wikipedia.org/wiki/MASCOT.

[40] NASA Space Science Data Coordinated Archive. *Asteroid 162173 Ryugu*. 2014. URL: https://en.wikipedia.org/wiki/162173_Ryugu.

[41] NASA Space Science Data Coordinated Archive. *OSIRIS-REx mission*. 2016. URL: https://en.wikipedia.org/wiki/OSIRIS-REx.

[42] NASA Space Science Data Coordinated Archive. *Asteroid 101955 Bennu*. 2016. URL: https://en.wikipedia.org/wiki/101955_Bennu.

[43] PeiJia Li et al. "Orbit determination for Chang'E-2 lunar probe and evaluation of lunar gravity models". In: *Science China Physics, Mechanics and Astronomy* 55.3 (2012), pp. 514–522.

[44] Christopher F Chyba. "The violent environment of the origin of life: progress and uncertainties". In: *Geochimica et Cosmochimica Acta* 57.14 (1993), pp. 3351–3358.

[45] Asteroid Mining Corporation. *What is AMC currently developing?* 2022. URL: https://asteroidminingcorporation.co.uk/.

[46] EM Galimov et al. "The Chelyabinsk fireball and meteorite: implications for asteroid hazard assessment". In: *Meteoritics and Planetary Science Supplement* 76 (2013), p. 5340.

[47] Pasquale Tricarico and Mark V Sykes. "The dynamical environment of Dawn at Vesta". In: *Planetary and Space Science* 58.12 (2010), pp. 1516–1525.

[48] Mark J Cintala, James W Head, and Lionel Wilson. "The nature and effects of impact cratering on small bodies." In: *Asteroids* (1979), pp. 579–600.

[49] KR Housen et al. "Regolith development and evolution on asteroids and the moon." In: *Asteroids* (1979), pp. 601–627.

[50] Leland E Cunningham. "On the computation of the spherical harmonic terms needed during the numerical integration of the orbital motion of an artificial satellite". In: *Celestial mechanics* 2.2 (1970), pp. 207–216.

[51] Ernest William Hobson. *The theory of spherical and ellipsoidal harmonics*. CUP Archive, 1931.

[52] B Fong Chao and David Parry Rubincam. "The gravitational field of Phobos". In: *Geophysical research letters* 16.8 (1989), pp. 859–862.

[53] CT Barnett. "Theoretical modeling of the magnetic and gravitational fields of an arbitrarily shaped three-dimensional body". In: *Geophysics* 41.6 (1976), pp. 1353–1364.

[54] Olivier Jamet and Emilie Thomas. "A linear algorithm for computing the spherical harmonic coefficients of the gravitational potential from a constant density polyhedron". In: *Proceedings of the second international GOCE user workshop, GOCE, The Geoid and Oceanography, ESA-ESRIN, Frascati, Italy, Citeseer*. Citeseer. 2004, pp. 8–10.

[55] Helmut Moritz. "LP Pellinen—Scientific Memories". In: *Geodesy and Physics of the Earth*. Springer, 1993, pp. 5–8.

[56] Bierly W. "An elementary treatise on fouriers series and spherical, cylindrical, and ellipsoidal harmonics". In: *Ginnan Company, London* (1897).

[57] Gunnar Bodvarsson. "A surface integral in potential theory". In: *Geophysics* 35.3 (1970), pp. 501–503.

[58] Garmier Romain and Barriot Jean-Pierre. "Ellipsoidal harmonic expansions of the gravitational potential: theory and application". In: *Celestial Mechanics and Dynamical Astronomy* 79.4 (2001), pp. 235–275.

[59] AR Dobrovolskis and Joseph A Burns. "Life near the Roche limit: Behavior of ejecta from satellites close to planets". In: *Icarus* 42.3 (1980), pp. 422–441.

[60] Darla German and Alan L Friedlander. "A simulation of orbits around asteroids using potential field modelling". In: *Spaceflight mechanics 1991* (1991), pp. 1183–1201.

[61] Daniel Jay Scheeres. "Dynamics about uniformly rotating triaxial ellipsoids: applications to asteroids". In: *Icarus* 110.2 (1994), pp. 225–238.

[62] Otto Rausenberger. *Lehrbuch der analytischen Mechanik*. Vol. 1. BG Teubner, 1893.

[63] Robert A Werner and Daniel J Scheeres. "Exterior gravitation of a polyhedron derived and compared with harmonic and mascon gravitation representations of asteroid 4769 Castalia". In: *Celestial Mechanics and Dynamical Astronomy* 65.3 (1996), pp. 313–344.

[64] Rene Forsberg. *A study of terrain reductions, density anomalies and geophysical inversion methods in gravity field modelling*. Tech. rep. Ohio State Univ Columbus Dept Of Geodetic Science and Surveying, 1984.

[65] S Petrovic. "Determination of the potential of homogeneous polyhedral bodies using line integrals". In: *Journal of Geodesy* 71.1 (1996), pp. 44–52.

[66] V Pohanka. "Optimum expression for computation of the gravity field of a homogeneous polyhedral body1". In: *Geophysical Prospecting* 36.7 (1988), pp. 733–751.

[67] Dimitrios Tsoulis and Sveto Petrovic. "On the singularities of the gravity field of a homogeneous polyhedral body". In: *Geophysics* 66.2 (2001), pp. 535–539.

[68] Daniel J Scheeres et al. "Orbits close to asteroid 4769 Castalia". In: *Icarus* 121.1 (1996), pp. 67–87.

[69] Daniel J Scheeres et al. "Dynamics of orbits close to asteroid 4179 Toutatis". In: *Icarus* 132.1 (1998), pp. 53–79.

[70] W Hu and Daniel Jay Scheeres. "Numerical determination of stability regions for orbital motion in uniformly rotating second degree and order gravity fields". In: *Planetary and Space Science* 52.8 (2004), pp. 685–692.

[71] P Antreasian et al. "Preliminary considerations for NEARs low-altitude passes and landing operations at 433 Eros". In: *AIAA/AAS Astrodynamics Specialist Conference and Exhibit*. 1998, p. 4397.

[72] DJ Scheeres, Bobby G Williams, and James K Miller. "Evaluation of the dynamic environment of an asteroid: Applications to 433 Eros". In: *Journal of Guidance, Control, and Dynamics* 23.3 (2000), pp. 466–475.

[73] Daniel Scheeres et al. "The actual dynamical environment about Itokawa". In: *AIAA/AAS Astrodynamics Specialist Conference and Exhibit*. 2006, p. 6661.

[74] Stephen B Broschart and Daniel J Scheeres. "Control of hovering spacecraft near small bodies: application to asteroid 25143 Itokawa". In: *Journal of Guidance, Control, and Dynamics* 28.2 (2005), pp. 343–354.

[75] PG Antreasian et al. "The design and navigation of the NEAR-Shoemaker landing on Eros". In: (2001).

[76] Gregory Lantoine et al. "1 Optimal trajectories for soft landing on asteroids". In: (2006).

[77] Hajime Yano et al. "Touchdown of the Hayabusa spacecraft at the Muses Sea on Itokawa". In: *Science* 312.5778 (2006), pp. 1350–1353.

[78] Matt Hawkins, Yanning Guo, and Bong Wie. "ZEM/ZEV feedback guidance application to fuel-efficient orbital maneuvers around an irregular-shaped asteroid". In: *AIAA Guidance, Navigation, and Control Conference*. 2012, p. 5045.

[79] CR Chapman et al. "Discovery and physical properties of Dactyl, a satellite of asteroid 243 Ida". In: *Nature* 374.6525 (1995), pp. 783–785.

[80] Derek C Richardson and Kevin J Walsh. "Binary minor planets". In: *Annu. Rev. Earth Planet. Sci.* 34 (2006), pp. 47–81.

[81] Daniel J Scheeres. "Stability in the full two-body problem". In: *Modern Celestial Mechanics: From Theory to Applications*. Springer, 2002, pp. 155–169.

[82] Eugene G Fahnestock and Daniel J Scheeres. "Simulation and analysis of the dynamics of binary near-Earth Asteroid (66391) 1999 KW4". In: *Icarus* 194.2 (2008), pp. 410–435.

[83] Julie Bellerose and DJ Scheeres. "Periodic orbits in the full two body problem". In: *AAS/Division of Dynamical Astronomy Meeting# 38*. Vol. 38. 2007, pp. 14–02.

[84] Andrzej J Maciejewski. "Reduction, relative equilibria and potential in the two rigid bodies problem". In: *Celestial Mechanics and Dynamical Astronomy* 63.1 (1995), pp. 1–28.

[85] N Borderies. "Mutual gravitational potential ofN solid bodies". In: *Celestial Mechanics* 18.3 (1978), pp. 295–307.

[86] Curt Von Braun. *On the gravitational potential of two arbitrary rotating bodies with applications to the Earth-Moon system*. The University of Texas at Austin, 1991.

[87] Paul Geissler et al. "Erosion and ejecta reaccretion on 243 Ida and its moon". In: *Icarus* 120.1 (1996), pp. 140–157.

[88] Joshua Ashenberg. "Proposed method for modeling the gravitational interaction between finite bodies". In: *Journal of Guidance, Control, and Dynamics* 28.4 (2005), pp. 768–774.

[89] Robert A Werner and Daniel J Scheeres. "Mutual potential of homogeneous polyhedra". In: *Celestial Mechanics and Dynamical Astronomy* 91.3 (2005), pp. 337–349.

[90] Eugene G Fahnestock and Daniel J Scheeres. "Simulation of the full two rigid body problem using polyhedral mutual potential and potential derivatives approach". In: *Celestial Mechanics and Dynamical Astronomy* 96.3 (2006), pp. 317–339.

[91] Eugene Fahnestock et al. "Polyhedral potential and variational integrator computation of the full two body problem". In: *AIAA/AAS Astrodynamics Specialist Conference and Exhibit*. 2006, p. 6289.

[92] Alfred S McEwen and Edward B Bierhaus. "The importance of secondary cratering to age constraints on planetary surfaces". In: *Annu. Rev. Earth Planet. Sci.* 34 (2006), pp. 535–567.

[93] A Mantz, R Sullivan, and J Veverka. "Regolith transport in craters on Eros". In: *Icarus* 167.1 (2004), pp. 197–203.

[94] PC Thomas et al. "The shape of Ida". In: *Icarus* 120.1 (1996), pp. 20–32.

[95] DJ Scheeres, DD Durda, and PE Geissler. "The fate of asteroid ejecta". In: *Asteroids III* 1 (2002), pp. 527–544.

[96] Andrew F Cheng et al. "Laser altimetry of small-scale features on 433 Eros from NEAR-Shoemaker". In: *Science* 292.5516 (2001), pp. 488–491.

[97] Douglas P Hamilton and Joseph A Burns. "Orbital stability zones about asteroids". In: *Icarus* 92.1 (1991), pp. 118–131.

[98] Douglas P Hamilton and Joseph A Burns. "Orbital stability zones about asteroids: II. The destabilizing effects of eccentric orbits and of solar radiation". In: *Icarus* 96.1 (1992), pp. 43–64.

[99] B Chauvineau and F Mignard. "Dynamics of binary asteroids: I. Hills case". In: *Icarus* 83.2 (1990), pp. 360–381.

[100] K Richter and HU Keller. "On the stability of dust particle orbits around cometary nuclei". In: *Icarus* 114.2 (1995), pp. 355–371.

[101] Douglas P Hamilton and Alexander V Krivov. "Dynamics of distant moons of asteroids". In: *Icarus* 128.1 (1997), pp. 241–249.

[102] B Chauvineau, P Farinella, and F Mignard. "Planar orbits about a triaxial body: Application to asteroidal satellites". In: *Icarus* 105.2 (1993), pp. 370–384.

[103] Daniel D Durda et al. "Detecting crater ejecta-blanket boundaries and constraining source crater regions for boulder tracks and elongated secondary craters on Eros". In: *Meteoritics & Planetary Science* 47.6 (2012), pp. 1087–1097.

[104] Katarina Miljkovic et al. "Morphology and population of binary asteroid impact craters". In: *Earth and Planetary Science Letters* 363 (2013), pp. 121–132.

[105] William F Bottke Jr and H Jay Melosh. "Binary asteroids and the formation of doublet craters". In: *Icarus* 124.2 (1996), pp. 372–391.

[106] Peter Halamek. *Motion in the potential field of a thin bar*. The University of Texas at Austin, 1988.

[107] AD Bruno. "On geometric methods in works by VI Arnold and VV Kozlov". In: *arXiv preprint arXiv:1401.6320* (2014).

[108] Andres Riaguas, Antonio Elipe, and Martin Lara. "Periodic orbits around a massive straight segment". In: *International Astronomical Union Colloquium*. Vol. 172. Cambridge University Press. 1999, pp. 169–178.

[109] Steven J Ostro et al. *Asteroid radar astronomy*. 2002.

[110] Yang Yu and Hexi Baoyin. "Orbital dynamics in the vicinity of asteroid 216 Kleopatra". In: *The Astronomical Journal* 143.3 (2012), p. 62.

[111] Yang Yu and Hexi Baoyin. "Resonant orbits in the vicinity of asteroid 216 Kleopatra". In: *Astrophysics and Space Science* 343.1 (2013), pp. 75–82.

[112] Yang Yu and Hexi Baoyin. "Generating families of 3D periodic orbits about asteroids". In: *Monthly Notices of the Royal Astronomical Society* 427.1 (2012), pp. 872–881.

[113] Jean-Luc Margot et al. "Binary asteroids in the near-Earth object population". In: *Science* 296.5572 (2002), pp. 1445–1448.

[114] Stephen M Slivan et al. "Spin vectors in the Koronis family: comprehensive results from two independent analyses of 213 rotation lightcurves". In: *Icarus* 162.2 (2003), pp. 285–307.

[115] Dan T Britt et al. "Asteroid density, porosity, and structure". In: (2003).

[116] J Veverka et al. "Dactyl: Galileo observations of Ida's satellite". In: *Icarus* 120.1 (1996), pp. 200–211.

[117] MJS Belton et al. "Bulk density of asteroid 243 Ida from the orbit of its satellite Dactyl". In: *Nature* 374.6525 (1995), pp. 785–788.

[118] David Vokrouhlicky, David Nesvorny, and William F Bottke. "The vector alignments of asteroid spins by thermal torques". In: *Nature* 425.6954 (2003), pp. 147–151.

[119] P Stooke. *NASA Planetary Data System Small Body Shape Models V1. 0.* Tech. rep. EAR-A-5-DDR-STOOKE-SHAPE-MODELS-V1. 0, 2002.

[120] Louis A D'Amario et al. "Galileo 1989 VEEGA trajectory design". In: *Journal of the Astronautical Sciences* 37 (1989), pp. 281–306.

[121] J Veverka et al. "Galileo's encounter with 951 Gaspra: Overview". In: *Icarus* 107.1 (1994), pp. 2–17.

[122] RP Binzel et al. "Asteroid 243 Ida: Groundbased photometry and a pre-Galileo physical model". In: *Icarus* 105.2 (1993), pp. 310–325.

[123] John L Africano et al. "Deep-space satellite observations using the near-Earth asteroid tracking (NEAT) camera at AMOS". In: *Multifrequency Electronic/Photonic Devices and Systems for Dual-Use Applications*. Vol. 4490. SPIE. 2001, pp. 187–193.

[124] Edward Bowell et al. "Asteroid orbit computation". In: *Asteroids III* 1 (2002), pp. 27–43.

[125] Chen Qiuli, Chen Zhonggui, and H Wang. "Method of modeling solar radiation pressure based on attitude control law of navigation satellites". In: *CSNC2013, Wuhan* (2013).

[126] Kevin J Walsh, Derek C Richardson, and Patrick Michel. "Rotational breakup as the origin of small binary asteroids". In: *Nature* 454.7201 (2008), pp. 188–191.

[127] Masatoshi Hirabayashi. "Failure modes and conditions of a cohesive, spherical body due to YORP spin-up". In: *Monthly Notices of the Royal Astronomical Society* 454.2 (2015), pp. 2249–2257.

[128] Yang Yu, Derek C Richardson, and Patrick Michel. "Structural analysis of rubble-pile asteroids applied to collisional evolution". In: *Astrodynamics* 1.1 (2017), pp. 57–69.

[129] Daniel J Scheeres. "Landslides and mass shedding on spinning spheroidal asteroids". In: *Icarus* 247 (2015), pp. 1–17.

[130] David Jewitt et al. "Disintegrating asteroid P/2013 R3". In: *The astrophysical journal letters* 784.1 (2014), p. L8.

[131] EM Rocco and LD Gonçalves. "Simulation of the trajectories described by a space vehicle around the asteroid 243 Ida and its natural satellite Dactyl". In: *Journal of Physics: Conference Series*. Vol. 911. 1. IOP Publishing. 2017, p. 012019.

[132] L Lan et al. "Motion of the moonlet in the binary system 243 Ida". In: *Acta Mechanica Sinica* 34.1 (2018), pp. 214–224.

[133] A Rossi, F Marzari, and P Farinella. "Orbital evolution around irregular bodies". In: *Earth, planets and space* 51.11 (1999), pp. 1173–1180.

[134] EW Hobson. "The theory of spherical and ellipsoidal harmonics, Chelsea Pub". In: *Co., New York* (1955).

[135] HG Walter. *Dynamics of Satellites*. 1969.

[136] Milos Pick, Jan Picha, and Vincenc Vyskocil. "Theory of the earth's gravity field". In: *Amsterdam; New York: Elsevier Scientific Pub. Co* (1973).

[137] D Dechambre and DJ Scheeres. "Transformation of spherical harmonic coefficients to ellipsoidal harmonic coefficients". In: *Astronomy & Astrophysics* 387.3 (2002), pp. 1114–1122.

[138] Robert A Werner. "The gravitational potential of a homogeneous polyhedron or don't cut corners". In: *Celestial Mechanics and Dynamical Astronomy* 59.3 (1994), pp. 253–278.

[139] William Boyce. "Comment on a formula for the gravitational harmonic coefficients of a triaxial ellipsoid". In: *Celestial Mechanics and Dynamical Astronomy* 67.2 (1997), pp. 107–110.

[140] Wei-Duo Hu and Daniel J Scheeres. "Periodic orbits in rotating second degree and order gravity fields". In: *Chinese Journal of Astronomy and Astrophysics* 8.1 (2008), p. 108.

[141] WD Hu, DJ Scheeres, and KH Xiang. "The characteristics of near asteroid orbital dynamics and its implication to mission analysis". In: *Progress in Astronomy* 27.2 (2009), pp. 152–166.

[142] H-t Cui et al. "Spacecraft motion analysis about slowly rotating small body". In: *ACTA AERONAUTICA ET ASTRONAUTICA SINICA-SERIES A AND B-* 25.1 (2004), pp. 16–20.

[143] PingYuan Cui et al. "Target selection and transfer trajectories design for exploring asteroid mission". In: *Science China Technological Sciences* 53.4 (2010), pp. 1150–1158.

[144] Sharyl M Byram, Daniel J Scheeres, and Michael R Combi. "Models for the comet dynamical environment". In: *Journal of Guidance, Control, and Dynamics* 30.5 (2007), pp. 1445–1454.

[145] Stephen B Broschart, Daniel J Scheeres, and Benjamin F Villac. "New families of multi-revolution terminator orbits near small bodies". In: *Advances in the Astronautical Sciences* 135.3 (2009), pp. 1685–1702.

[146] P Vallabh Sharma. "Rapid computation of magnetic anomalies and demagnetization effects caused by bodies of arbitrary shape". In: *Pure and Applied Geophysics* 64.1 (1966), pp. 89–109.

[147] MK Paul. "The gravity effect of a homogeneous polyhedron for three-dimensional interpretation". In: *Pure and Applied Geophysics* 112.3 (1974), pp. 553–561.

[148] Hans-Jürgen Götze. "Ein numerisches Verfahren zur Berechnung der gravimetrischen und magnetischen Feldgrößen für dreidimensionale Modellkörper". PhD thesis. Technische Universität Clausthal, 1976.

[149] Jörg Waldvogel. "The Newtonian potential of homogeneous polyhedra". In: *Zeitschrift für angewandte Mathematik und Physik ZAMP* 30.2 (1979), pp. 388–398.

[150] H-J Götze and Bernd Lahmeyer. "Application of three-dimensional interactive modeling in gravity and magnetics". In: *Geophysics* 53.8 (1988), pp. 1096–1108.

[151] VN Strakhov, MI Lapina, and AB Yefimov. "A solution to forward problems in gravity and magnetism with new analytical expressions for the field elements of standard approximating bodies I. Izvestiya". In: *Earth sciences* 22.6 (1986), pp. 471–482.

[152] VN Strakhov, MI Lapina, and AB Yefimov. "Solution of direct gravity and magnetic problems with new analytical expressions of the field of typical approximating bodies II". In: *Izvestiya, Earth Sciences* 22 (1986), pp. 566–575.

[153] H Holstein and B Ketteridge. *Gravimetric analysis of uniform polyhedra: Geophysics*. 1996.

[154] M Okabe. "Analytical expressions for gravity anomalies due to homogeneous polyhedral bodies and translations into magnetic anomalies". In: *Geophysics* 44.4 (1979), pp. 730–741.

[155] Patrick T Wittick and Ryan P Russell. "Mascon models for small body gravity fields". In: *AAS/AIAA Astrodynamics Specialist Conference*. Vol. 162. 2017, pp. 17–162.

[156] Aleksandr Danilovich Aleksandrov, Mikhail Alekseevich Lavrent'ev, et al. *Mathematics: its content, methods and meaning*. Courier Corporation, 1999.

[157] Murray R Spiegel. *Theory and problems of vector analysis and an introduction to tensor analysis*. Tech. rep. 1959.

[158] W Gellert. *Kleine Enzyklopädie Mathematik: Deutsch Verlag*. 1977.

[159] Dimitrios Tsoulis. "Analytical and numerical methods in gravity field modeling of ideal and real masses". In: *Deutsche Geodätische Kommission, Reihe C* Heft Nr 510 (1999).

[160] Dimitrios Tsoulis. "Analytical computation of the full gravity tensor of a homogeneous arbitrarily shaped polyhedral source using line integrals". In: *Geophysics* 77.2 (2012), F1–F11.

[161] C Bradford Barber, David P Dobkin, and Hannu Huhdanpaa. "The quickhull algorithm for convex hulls". In: *ACM Transactions on Mathematical Software (TOMS)* 22.4 (1996), pp. 469–483.

[162] VK Abalakin et al. "Report of the IAU/IAG working group on cartographic coordinates and rotational elements of the planets and satellites: 2000". In: *Celestial Mechanics and Dynamical Astronomy* 82.1 (2002), pp. 83–111.

[163] PETR Pravec, Alan W Harris, and Tadeusz Michalowski. "Asteroid rotations". In: *Asteroids III* 113 (2002).

[164] Yu Jiang et al. "Orbits and manifolds near the equilibrium points around a rotating asteroid". In: *Astrophysics and Space Science* 349.1 (2014), pp. 83–106.

[165] Yu Jiang et al. "Order and chaos near equilibrium points in the potential of rotating highly irregular-shaped celestial bodies". In: *Nonlinear Dynamics* 83.1 (2016), pp. 231–252.

[166] Yu Jiang and Hexi Baoyin. "Annihilation of relative equilibria in the gravitational field of irregular-shaped minor celestial bodies". In: *Planetary and Space Science* 161 (2018), pp. 107–136.

[167] GA Tsirogiannis, EA Perdios, and VV Markellos. “Improved grid search method: an efficient tool for global computation of periodic orbits”. In: *Celestial Mechanics and Dynamical Astronomy* 103.1 (2009), pp. 49–78.